

We respond below to the comments raised by the reviewer, setting his words in *italics* with our response following below.

## Response to Referee 1 (Volwerk)

*This paper discusses a fundamental plasmaphysical phenomenon: the ion acoustic wave, specifically the electric current-driven ion acoustic wave. Here, the current is defined as a velocity difference between the ions and the electrons in the ion rest frame. The authors use the RPC data from one close flyby of Rosetta by comet 67P/CG. They find the waves from just before closest approach to the comet and during egress up to a certain point. The “sudden” start is due to instrument operations the end is because of a quenching of the instability. The authors try to use the data from the different RPC instruments to characterize the plasma environment, but find that, because of instrumental limitations (e.g. spacecraft charging) not all particle distribution functions can be obtained. After realistic assumptions on how to interpret the particle data, several different setups are made to calculate the dispersion relation of the ion acoustic waves. The authors show that one of the  $\gamma/2$  scenarios works best to explain the observations.*

*This paper is well written, with the minor “complaint” that everything is well described in detail, but the authors do not spend any time of introducing the instability itself, although there are several citations to various papers (also by the lead author). It would be nice, for the interested reader, if the authors would add one short section on the specific instability.*

*However, I am not entirely sure how to interpret this paper, I have the feeling that there is more than just showing that the ion acoustic model can be described. Is it also the purpose of the authors to show that the observations of these waves can be a method to sample a parameter space of the plasma populations that cannot be measured by a charged spacecraft? If this is indeed the case (and it would be very useful) then this should be brought more forward, also in the abstract of the paper.*

We have included more discussion on how the combination of wave observations and theory supplements the other measurements in the discussion section and also in the abstract. We have put some information on the current-driven ion acoustic instability in the introduction – next to where ion acoustic waves are mentioned.

*On line 169: “the wave frequency does not follow . . .” I would add here “of the observed waves” otherwise it reads a little confusing with the previous sentences talking about cyclotron waves.*

Changed as suggested. We also inserted a sentence giving specific numbers in response to the other referee.

*On page 9 I am having trouble understanding the statement: “Cold ions are picked up by the electric field, moving along trajectories with a radius of curvature that is even larger.” With the high density of the plasma that is measured*

*by MIP, would this not mean that the spacecraft is in a pile-up region ( $B \sim 30$  nT) and thus the solar wind has been braked significantly. How much slow down do the authors expect? With 30 vs 5 nT, the “solar wind velocity” would probably be a factor 6 slower. What would the expected gyro radius be, then?*

Assuming an initial speed of 400 km/s, slowed down by a factor of 6, the gyro radius of an  $\text{H}_2\text{O}^+$  ion in a 30 nT magnetic field would be 415 km, which is “even larger” than the 50 km found from the warm ion thermal speed.

*Line 225: “found to similar to the difference” here “be” is missing.*

Corrected.

*Line 234: “Examining the magnetic field in Fig. 2 we see no large scale change near 18:00, which means that there was no large scale current present.” I am not sure that is correct. The magnetic field remains the same, if suddenly a large scale current would disappear (the one driving the IA waves) then would one not likely see a change in the magnetic field, like just before 21:00?*

It seems this statement can be misunderstood. A change, as for example the disappearance of a large scale current, would indeed be seen in the magnetic field. We have replaced the sentence by the following (the first half of the original sentence still remains), which we think should be clearer:

“That the field remains constant, except for small fluctuations, while the spacecraft moves means that there is no large scale magnetic field gradient in this region and hence no large scale current either. ”

*Line 266: Here Fig. 8b is discussed, and it would be good if the authors would put in that that is for the outbound part of the orbit.*

We have inserted the following clause at the beginning of the first sentence of the paragraph:

“For the outbound part of the spacecraft trajectory,”

We respond below to the comments raised by the reviewer, setting the reviewer's words in *italics* with our response following below.

## Response to Referee 2

*This paper addresses observations of ion acoustic waves (IAW) in the vicinity of 67P nucleus a few months before perihelion. The paper is based on observations of 4 instruments of the Rosetta Plasma Consortium and of ROSINA-COPS. The IAW are observed in the region of high current drift (near closest approach to the nucleus) in connection with high current drift, while they were not further from the nucleus where there was no significant current drift observed.*

*The paper is in general written in good style, but the formulation of physical processes is sometimes more qualitative than quantitative, even vague at times. The identification of the IAW lacks clear characterization of their properties. Some numbers of the observed or derived parameters are given but not always substantiated.*

*Reference is made to the first detection paper of IAW at 67P. The detection conditions, including the plasma parameters seem to be different, but those differences, and their consequences on the IAW properties may not be discussed in depth.*

We have amended the manuscript, and we think that it now adequately describes how the ion acoustic waves were identified, that the derived parameters are sufficiently substantiated.

*Beyond the plasma physics interest of the detection of IAW in 67P environment, in the discussion, I would like to see a short paragraph discussing the interest of the detection of IAW in terms of cometary physics and cometary sciences. As written in the first sentence in the introduction, "observations of waves can give us information of the plasma physics in which they are generated and through which they have travelled" (a rather strange formulation by the way). In the discussion I would have expected reading something of what the detection and characterization of IAW bring in terms of understanding the comet plasma (and neutral ?) environment how do they help in constraining physical processes at work inside the coma.*

*The abstract may not fully reflect the content of the paper. It should include something on:*

- Hot ions are not contributing to the IAW*
- IAW waves are detected when a current flow is present as determined from B-field measurements*
- The high spacecraft charging complicates the interpretation of the observations.*

We have put all those things in the abstract, and we have also added text to the discussion section to highlight how wave observations in combination with wave theory supplement the measurements by the other instruments and the interpretation thereof.

*Line 10. Replace « travelled » by « propagated » ?*

Changed as suggested.

*Line 12: Add “charged” in front of “particle”*

Changed as suggested.

*It’s hard to appreciate the importance of the Doppler shift without the mentioning of the frequency range of the waves. Explain the relation between the bulk velocity and the Doppler shift.*

This must be referring to the mentioning of the Doppler shift in the abstract. We have modified the sentence in questions so that it also states the frequency range of the waves in the plasma frame.

“Near closest approach the propagation direction was within  $50^\circ$  from the direction of the bulk velocity, leading to a Doppler shift of the waves, which in the plasma frame appear below the ion plasma frequency  $f_{pi} \approx 2\text{kHz}$ , to the spacecraft frame where they cover a frequency range up to approximately  $4\text{kHz}$ .”

*Line 21: Provide the parameters that lead to a  $LHF < 15\text{ Hz}$ .*

The reader is referred to the original papers by Andre et al (2017) and Karlsson et al. (2017) for further details. The purpose of the introduction is merely to provide context so that the present work can be located in the greater scheme of things and to briefly review the relevant history of the field, which in this case concerns other observations by Rosetta, mostly but not only wave observations.

*Line 23-26: Is there a relation between the steepened waves only observed outside the diamagnetic cavity and the waves in the LHF range observed on both sides*

Stenberg Wieser et al. (2017) reported that they appear in the same position at the same time outside of the cavity. One may speculate about how energy is transferred between different wave modes and between different parts of the comet environment, but the present paper is hardly the place for that.

*At this stage, it would be useful to recall how IAW modes are identified. During the review, I just came across recently published paper (that was not available at the time of the paper submission) that addresses well the identification of IAW modes (Mozer et al. 2020). One characteristic used is the phase. Can information about the phase be obtained with the LAP probe signal ?. Would the availability of both P1 and P2 signals (although with different amplitudes) help in obtaining information about the phase?*

We added the following text:

“Ion acoustic waves can be identified by measuring either the variations in plasma density or in the electric field. At comet 67P/Churyumov-Gerasimenko, Gunell et al. (2017b) detected the waves in electric field oscillations and Gunell et al. (2017a) in density variations. In this work, the detection relies on density variations.”

As to the suggestion about adopting the method of Mozer et al. (2020), those authors measured two components of the electric field, using four probes, and computed the phase difference between those two electric field components. This enabled them to assess the polarisation of the wave. Rosetta does not have four probes. During the observations reported here, probe 1 measured the density variations (see also the answer to one of the comments below), whereas the negatively biased probe 2 recorded a displacement current or possibly a combination of a displacement current and an ion current. Thus, the two probes recorded vastly different quantities, and the electric field polarisation cannot be addressed with the methods used by Mozer et al. (2020). A comet-bound spacecraft equipped with four, or better six, probes would of course be vastly superior, but that is not the spacecraft that we have.

*Line 28: Define undefined variables, e.g.  $\omega$ ,  $k$ ,  $k_B$ ,  $m_i$ . The need to define variables used applies also to other parts of the manuscript.*

Definitions have been added.

*Line 33-40. It is said that no diamagnetic cavity was seen during the flyby studied,. The plasma conditions, and characteristics of the IAW confined in the diamagnetic cavity (Gunell et al, 2017) seem to be somewhat different from those reported in this article (no diamagnetic cavity had formed). There is no discussion of the similarities and differences between the two studies.*

In response to both this and the comment after next we added the following text to the end of the introduction:

“Thus, the spacecraft was situated in the inner coma, where the plasma was of cometary origin. The plasma parameters, although not exactly the same, were in a range similar to that of the diamagnetic cavity observations near perihelion. The magnetic field environment was dominated by magnetic pileup and draping during the flyby, while the diamagnetic cavity has its own peculiar magnetic field environment with a sharp discontinuity at the boundary.”

*Line 41: “likely” is a vague statement. Could it be that the cavity had formed closer to the nucleus, where the s/c did not go on that flyby ?.*

It is unlikely that it had formed based on an analysis by Goetz et al. (2016a). We have put the citation in at the end of the statement for justification.

*Line 43: explain the implication of the infant bow shock (from simulation) and the fact that the diamagnetic cavity had not formed (or was not observed).*

See our response to the comments two comments above of this.

*Line 46: Not sure CSEQ is known to all potential readers. A reference, beyond the definition that follows, would be desirable.*

The original definition comes from the SPICE kernel. We added this and a reference to Acton (1996).

*Line 56: replace “plasma waves” by “probe current variations attributed to waves”*

Changed as suggested.

*Line 57: clarify how the probe current variation relates to plasma waves*

This is discussed in the second paragraph of Sect. 2.2.

*Line 59: You may not have said before that there were two Langmuir Probes*

We inserted the following sentence a little bit above:

“RPC-LAP is constituted of two spherical probes, 5 cm in diameter, that are mounted on booms protruding from the spacecraft.”

*Line 61: It would be useful to indicate the value of the S/C potential, in order to better appreciate the difference between a probe at +30 V and one at -30V.*

The spacecraft potential was approximately  $-20$  V. We have added this piece information to the text.

*Line 62: Was the bulk speed of the ions “measured” or “estimated”? See further questions later*

We have changed to “derived”.

*Line 67: add “magnetic field” in “The (magnetic field) components”*

Changed as suggested.

Figure 2:

*Would be useful to say in the legend or to write in the top two panels the bias value for each of the two LAP probes.*

We have put that piece of information in the figure caption.

*Is there a physical explanation for the sharp transition of the plasma density derived from MIP measurements before and after 10:00 while the RPC-ICA spectra are quite similar. Any explanation as to why there are no RPC-MIP measurements after 20:00?*

Trying to estimate the plasma density from RPC-ICA spectra is not advisable under circumstances where the spacecraft is not negative enough to allow more than a small fraction of the ions can be detected by RPC-ICA (see also the reply to your comment further below about the invisibility of the cold ions). After 20:00 the density falls under the detection limit for the RPC-MIP Short Debye Length mode.

*Legend: I would say the plasma density is “derived” rather than “measured” from the RPC-MIP measurements.*

Changed as suggested.

*Line 73-74: Not obvious in the figure that the frequency scale starts at 200 Hz. Setting the origin of the Y-scale at 0 and leaving the space between 0 and 200 Hz blank would make it clear.*

The information is stated in the figure caption.

*Line 75: Not clear if signal is a wave signal or noise enhancement. It would be useful to show the non-Doppler shifted LHF line for reference*

The lower hybrid frequency is far below the lower limit of the frequency range shown. Estimated at closest approach the lower hybrid frequency is

$$f_{\text{lh}} = \frac{f_{\text{pi}}}{\sqrt{1 + f_{\text{pe}}^2/f_{\text{ce}}^2}} \approx \frac{2.0 \text{ kHz}}{\sqrt{1 + \left(\frac{360 \text{ kHz}}{1.0 \text{ kHz}}\right)^2}} \approx 6 \text{ Hz}$$

*Line 77-78. I would put it the other way around. Probe 1 being dominated by electron current, and probe 2 being dominated by ion current, leads to the fact that the power spectral density of probe 1 is several orders of magnitude higher.*

It is written in this way, because it answers your next question about why the variations in probe current are proportional to the the density variation of the wave.

*Line 77: clarify « . . . . signal proportional to the density variation of the waves » should be substantiated*

For increased clarity we have inserted a new sentence, mentioning the two different regimes, which of these the present measurements adhere to, and indicating where this matter is discussed in more detail:

“The probe operated in this regime also in the previously published observations of waves in the diamagnetic cavity (Gunell et al., 2017a), whereas in the first published observations (Gunell et al., 2017b), the probe was capacitively coupled to the plasma. A simple test to distinguish between the two regimes is to measure the wave amplitude as a function of probe bias, where a negatively biased probe suppresses the particle current (Torvén et al., 1995). In the present case, we compare the two probes that are biased differently (see also Gunell et al., 2017b).”

*Explain why the wave signal observed is identified as IAW. What are the wave characteristics that allow to infer that?*

We have added the following sentence at the end of the first paragraph of Sect. 2.2:

“The waves are identified as ion acoustic waves, because they are compressional, showing a plasma density variation, and other wave modes can be excluded for the spatial and temporal scales where they are observed as shown in Sect. 2.4.”

*Line 80: This statement about the plasma density being comparable in both events is not verifiable as the density measurements are not illustrated in Fig. 3 of the 2017 paper.*

The density is illustrated in both the 2017 papers: in Fig. 1 of (Gunell et al. 2017a). In (Gunell et al. 2017b) there is an entire section on density estimates, including an illustration in Fig. 5 of values obtained from different instruments, and there is a table of values that were used in the computations in that paper. There is also an assessment of the results of those computations and what that implies for the tabulated values. All of this confirms the statement made in the present paper.

*Line 82: Clarify “condition when signal is observed through displacement current (capacitive coupling) vs particle current? If I understand well, a decrease of a factor of 10 of the current implies that the wave can no more be detected by the current variation, but instead by capacity coupling. This statement should be elaborated.*

The clarification to the question above answers this question too:

“The probe operated in this regime also in the previously published observations of waves in the diamagnetic cavity (Gunell et al., 2017a), whereas in the first published observations (Gunell et al., 2017b), the probe was capacitively coupled to the plasma. A simple test to distinguish between the two regimes is to measure the wave amplitude as a function of probe bias, where a negatively biased probe suppresses the particle current (Torvén et al., 1995). In the present case, we compare the two probes that are biased differently (see also Gunell et al., 2017b).”

*Line 97: Provide the reference to the publication for the artefacts ? It seems that the artefacts are harmonics of 1 kHz as well evidenced in the PDS line at 19:08:54. This is within the range of the  $f_{ce}$  value given in line 168. Can it be excluded that those “artefacts” are harmonics of  $f_{ce}$ . It would be desirable to provide the value of  $f_{ce}$  for the period. Can it be ruled out that part of the detected noise is enhanced (excited) by those artefacts ? Are those artefacts discernable in the P2 data?*

The artefacts were also seen in the diamagnetic cavity (Gunell et al., 2017a). These are not harmonics of the electron cyclotron frequency, because the frequencies of the artefacts are constant throughout the day, while  $|\mathbf{B}|$ , to which  $f_{ce}$  is proportional, varies by about a factor of two. Examples of  $f_{ce}$  within the range in which it varies are now provided in Sect. 2.4. As seen in figure 2a the amplitude of the artefacts is significantly below that of the wave signal until that signal starts to fade away. The artefact may excite a low amplitude wave at the isolated frequencies where they are seen, but not the much higher amplitude waves of interest here, which also are present in a much wider frequency range than the artefacts. See also the figure next to this piece of text (Fig. A) for two time series of the probe current.

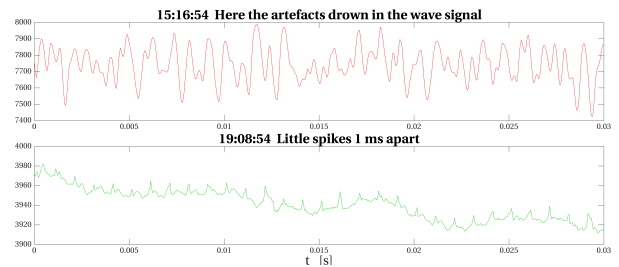


**Figure A:** Time series of the probe currents for two times during the day of 28 March 2015.

*Line 101-102: How do you quantify plasma inhomogeneities at 10%. What is the accuracy of the MIP measurements?*

See the electron density plot to the right. The accuracy of the data in the figure is  $5\text{--}10\text{ cm}^{-3}$ , the variations are one order of magnitude larger, and the mean is larger by yet another order of magnitude. The accuracy of the MIP measurements is also about 10%. The accuracy of the electron density from the MIP measurement is computed from the frequency resolution of the instrument, which measures the plasma frequency from the identification of the plasma frequency line in the mutual impedance spectra.

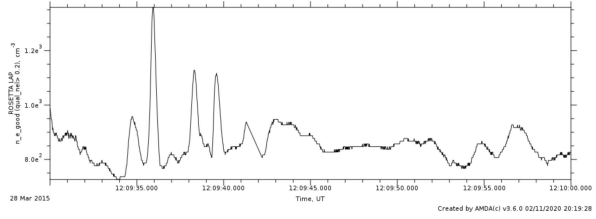


**Figure B:** LAP plasma density sample figure for this day.

*Line 104-105: Process by which the ions are getting heated (6eV) and how this temperature is derived?*

We merely observe those ions. The heating process is outside the scope of this paper. The temperature is obtained from the same fit that gave the density, mentioned a few lines below. We have introduced words to say that the temperature is also obtained by fitting.

*Line 105: You should say at least once that those are positive ions. Apologies if it was said before and I missed it.*

We inserted the word positive before ions in the first sentence of this paragraph. In other places in the manuscript we assume the ions to be  $\text{H}_2\text{O}^+$  ions.

*Are there also negative ions present in the plasma? if yes, how would those negative ions affect the IAW generation and damping ?*

There are no significant amounts of negative ions in the plasma, at least not from a plasma physics point of view. Measurements at comet 1P showed that fewer than one ion in  $10^4$  are negative.

*Line 107. I suppose the fit is performed with a drifting maxwellian population. Please confirm*

Confirmed. We updated the text to say “drifting Maxwellian”.

*Line 110-115. I Not convincing argument as to why most of the ion population is not visible, all ions (warm and cold) should be accelerated by the S/C potential, should they not ?*

*I have difficulties to follow the reasoning about the non-detectability of the cold ions. Should they not be accelerated to 20 V as well. If the fraction of that population that is detected may not be distinguishable from the ions belonging to the warm population, should they not appear in the maxwellian fit described earlier. This seems to be somewhat in contradiction when saying that it may explain that the cold water ion population (still accelerated to 20 V) is invisible to RPC-ICA. “May” means that there could be other explanations. Please elaborate.*

They are accelerated by the spacecraft potential, but the ability of the instrument to detect low energy ions is severely limited. The sensitivity of the detector is low for such low energies, and the angular range that allows entry into the instrument narrow. Thus, a mono-energetic low energy beam, which the cold ion population is, can go completely undetected. We described that in terms of a field of view, vanishing at low energies. This description seems to be inefficient as a form of communication, and we have changed the text to provide a better explanation.

“The sensitivity of RPC-ICA is low in the lowest energy range, and the angular range that allows entry into the instrument is narrow. A mono-energetic low energy beam is liable to be undetected. Thus, the discrepancy between the RPC-ICA measured ion density and the plasma density measured by RPC-MIP is explained by a cold water ion distribution that is invisible to RPC-ICA.”

Finally, to avoid misunderstanding, of course the Maxwellian fit is to the part of the distribution that is above the limit for detection.

*Line 116: Clarify how the various photoemission current is taken into account in the ion part of the I-V curve.*

The photoemission comes in as an offset in the ion current (below the plasma potential), and as such, does not play a role in the slope of the ion current. Also, LAP1 is in shadow behind the spacecraft for the first sweep. We added the following at the end of the paragraph:

“Photo emission comes in as an offset in the ion current, below the plasma potential, and as such, does not play a role in the slope of the ion current. Furthermore, for the first of the sweeps, the probe was in shadow behind the spacecraft.”

*Line 116: Discuss the deviation from linearity of the ion portion of the I-V curve at negative potential clearly visible at 13:25:26, but also discernable at 17:52:06. It is said earlier that the I-V curve is acquired in the -30 +30 V range. If so, it would be interesting to show the hidden part of the curve, between -30 V and -30 V.*

It is possible that the deviation from linearity is the onset of secondary emission from ion impact. However, it is not always present, does not behave very similarly from sweep to sweep, is sometimes non-linear and wavelike in nature, As a full Langmuir probe sweep takes 3.2 seconds, (i.e. is not instantaneous), it is more likely that this is a capacitive coupling to some excited wave propagated by ions with an observed frequency near 1 Hz and grows larger in amplitude when more ions are attracted by the probe. This is also confirmed to be present when looking at the continuous (60 Hz) ion current data from LAP 2. Therefore, we restrict the ion current fit to a region below the spacecraft potential where the ion current is linear, and any wave amplitude is small. A figure showing the “hidden” part is shown here (Fig. C). The figure in the paper has also been

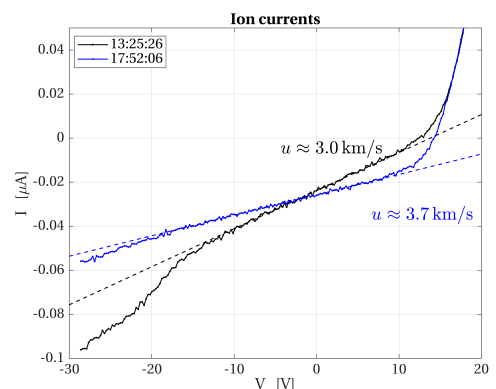


**Figure C:** LAP characteristics starting from the beginning of the sweep.

updated but in a different way with some new panels.

*My examination of the I-V curve indicates that the local plasma potential is about 20 V, confirming that the S/C is charged to about -20V. The energy of the ions hitting the probe may reach 50 V (60 V if the probe is polarized at -30 V). In this energy range, is it possible that secondary emission plays a role? is photoemission of the probe surface taken into account in the probe current ?*

We have reexamined the I-V curve and agree with the local plasma potential and spacecraft potential estimation.

Regarding secondary emission, it is certainly possible, but the quantum yield of ion impact ionisation is low for metals particularly at low energies, less than unity. And for a ceramic surface layer like TiN, it is likely that the quantum yield is even lower. We have added a sentence explaining that if secondary emission is present also at the low (10eV) energy range where our ion current analysis begins, then this would inflate our ion velocities with a factor equal 1+ the quantum yield. It would only have a very limited impact on Probe current variations attributed to waves.

Regarding photoemission, the LAP1 is in shadow between 11 and 14:30 and is not photoemitting. Also, at the potentials the ion current analysis is performed, the photoemission is an offset, and does not play a role in determining the effective ion speed.

*In eq (1), define variable  $V$ . Is such a formula directly applicable for a drifting ion population?. The hot ion population does not seem to be considered in the overall ion current. Justify. Discuss the applicability of eq (1) to the current plasma conditions*

The variable  $V$ , representing the probe to plasma potential, was already defined above the equation together with the bulk speed  $u$  and the current  $I$ . The warm ion population is neglected because of its low density, and the equation is applicable because the thermal speed of the cold ions is far below their bulk speed. A sentence to that effect has been introduced just before Eq. (1).

*Taking the ion density equal to the plasma density ignores the hot ion population contribution. Is this justified?*

Yes, it is. The warm ion density is  $4\text{cm}^{-3}$  and the plasma density  $1600\text{cm}^{-3}$ . The factor of 400 between them ensures that the error is negligible.

*A formulation of the I-V curve taking into account all current contributions should be written.*

With the changes made outlined above, we feel that all relevant current contributions have been described.

*A proper discussion of the various measurement uncertainties would be desirable*

We answer this now and refer back here, whenever this comment reappears below. We have written a new section about the uncertainties. We have not removed any existing

discussions from the other section, which leads to some overlap, but we don't find that overly troubling. The new section appears at Sect. 2.5 in the revised manuscript.

*Probably not surprising that the numbers are within the range of those observed by Odelstad et al. (2018) if the same method of analysis is used (I did not check that point). Point to be clarified.*

We do not claim it to be surprising. However, since the observations by Odelstad et al. (2018) were performed in a different magnetic field environment and at a different distance to the nucleus, it was no certainty beforehand that the results would be similar. We have added text, clarifying the different conditions.

*Line 126: Replace “ a upper “ with “an upper”*

The sentence has been removed in its entirety as, under careful examination, it has been found to be incorrect.

*Line 129: Not clear why the Biver et al 0.02 eV neutral temperature is compared to the 1eV (ion) kinetic energy. Please elaborate the argument.*

We added the sentence

“This confirms the assumptions stated above Eq. (1) and ensures the applicability of the equation.”

*Line 136. The slope of the two electron current curves are clearly different. Why do they provide the same value of Te (about 0.2 eV)?*

As the slope is proportional to both electron density and electron temperature, two different slopes measured at plasmas with different densities can have the same temperature. Also, for the temperatures obtained here, the values 0.16 and 0.22 were both rounded off to 0.2.

*Not clear how the plasma potential is estimated to 12 and 14 volts. Elaborate. My estimation is more around 20 V (see above). In fact, the plasma potential is derived from a measurement made inside the plasma sheath of the charged spacecraft. Discuss the uncertainty of this value?*

We have made a new assessment of the plasma potential, and also of the warm electron temperature. The new version of the manuscript says that the plasma potential is approximately 20 V and the warm electron temperature  $k_{\text{B}}T_{\text{ew}} = 2 \text{ eV}$ .

*When revising the paper, I would advice to discuss this spacecraft charging effects with reference to the recently published paper by Johansson et al. <https://doi.org/10.1051/0004-6361/202038592>*

We have added the following sentence in connection with the determination of the spacecraft potential.

“It was shown in simulations by Johansson et al. (2020) that the spacecraft potential is driven negative by positively biased elements on the solar panels that collect cold electrons from the plasma.”

*Discuss uncertainties in the derived numbers*

See our response to this comment on page 9.

*Line 143: Confirm that, in the presence of two equal-density electron populations, the MIP max represents the plasma frequency (how is it defined with two such different populations). It is noted that the MIP phase data are not referred to. Are they consistent with the amplitude data?*

In the presence of two electron populations (for instance two equal-density electron populations), the main resonance in the mutual impedance spectra is indeed associated to the (total) electron density, and give therefore access to the total electron density. In some cases (e.g. large temperature ratio and similar densities such as for two equal-density electron populations) a second resonance associated to electron acoustic waves generated in the plasma by the MIP electric transmitter. The general instrumental response of the MIP mutual impedance probe in a plasma characterised by two electron populations with different temperatures is described in Gilet et al. 2017 <<https://doi.org/10.1002/2017RS006294>> and Wattieaux et al, 2020 <<https://doi.org/10.1051/0004-6361/202037571>>. We have added the following sentence to the manuscript:

“The general instrumental response of the RPC-MIP mutual impedance probe in a plasma characterised by two electron populations with different temperatures is described by Gilet et al. (2017) and Wattieaux et al. (2020).”

*Line 162-163: What is the implication of the measurement uncertainty expressed by the sentence “Thus, the current density may have been both higher and lower than these average values during the flyby” ?*

See our response to this comment on page 9.

*Line 169: How is the wave frequency characterized? justify the important affirmation that the wave frequency does not follow the change of the magnetic field, used to justify that the waves observed are not electron cyclotron waves. Provide values.*

We inserted the following sentence to provide values:

“For example, the PSD peaks at 700 Hz for both times 13:24:54 and 15:16:54, shown by the black and red curves in Fig. 3, respectively, even though the electron cyclotron frequency was 1.1 kHz at 13:24:54 and 0.57 kHz at 15:16:54.”

*Line 172: How was the “typical length” for the variation in wave amplitude deduced to 10 km ?. What is meant by “typical length”*

This is described in the sentence immediately before the one where the word “typical” appears:

“The spacecraft was at 15 km cometocentric distance at closest approach and at 25 km at 18:00 when the wave amplitude started to decrease. Thus, the typical length for the variation in wave amplitude is about 10 km.”

*Line 177: clarify if you refer to electron or ion gyro-radius, or both*

We have replaced “particles” by “electrons and ions”.

*Table 1: Clarify parameters used. Electron VD?*

We added an explanation of the notation to the table caption.

*Line 184: the uncertainties in the measurements is not well reflected in the values reported in sect; 2. Can the measurement uncertainties be quantified?*

See our response to this comment on page 9.

*Line 190 -192 It would be desirable to provide the formula of the dispersion relation used, although indeed, proper reference is given. May be as important, if not more, than the formula for the distribution function.*

We have updated the text to provide that, but since this is somewhat involved and requires new notation to be introduced and several equations to be displayed, we have put it in a new appendix, which is now Appendix A.

*Line 194: define variable  $v$ ? is variable “ $vd$ ” used in the formula the same as “ $vD$ ” used in the table ? use consistent notation.*

$v$  means velocity. This piece of information has now been added to the manuscript. We have also changed all instances of  $v_d$   $v_D$ .

*Line 211: The non-effect of the warm ions (the one detected by ICA) lead to consider the cold ions whose density is set equal to the « measured » electron density. This makes a strong assumption that the plasma is locally neutral, which may not be the case in the sheath around the spacecraft. Justify.*

That the warm ions, due to their low density, have no influence on the wave properties does not tell us anything about the neutrality of the plasma. Also, the probe is outside the sheath as the Debye length, as estimated below, is only 26 cm.

*Line 214: is it justified to assign a drift velocity to only one of the two electron populations?*

As collisions cools the electrons to give them different temperatures they can also obtain different velocities. However, this comment inspired another test, namely assigning equal drift velocities to both electron population. This is now distribution 9. The result is reported in the revised manuscript:

“In distribution 9 the current is carried by both electron populations, which each are given a drift velocity of  $|\mathbf{v}_D| = 19.6 \text{ km s}^{-1}$ . This yields a lower growth rate than for distribution 2, but the mode is still unstable for a range of  $k$  values.”

Distribution 9 is now also included in Fig. 8 and the discussion thereof (see the revised manuscript).

*Line 216: Such a strong conclusion should be more substantiated.*

Following the evaluation of distribution 9 this statement has been moderated:

“We conclude that to drive the ion acoustic waves unstable the current cannot be carried by the warm electrons alone.”

This is substantiated by the computations based on distribution 9.

*Line 225: word missing: « ... is found to (be) similar.. »*

Corrected. Thanks also to referee 1.

*Line 245-248, and legend Fig 8: The notations used should be all defined (in the legend)*

Notation explanation may now be found in the caption.

*Line 250-251: Not clear what means a « reasonable spectrum » and how this observation is reached.*

“reasonable spectrum” is replaced by

“an interpretation in which observations and theory are consistent. This is explained in what follows”

*Line 251-273: The narrative discussions seem to be very qualitative. Not clear that the conclusions reached are well substantiated.*

The approach employed is to assess the observations and compare those to theory to the extent the measurements allow. To that extent they are well substantiated. For example we are only able to confine propagation angles to a rather wide range, and we cannot give precise numbers, as that indeed would be unfounded in fact.

*Line 275: specify that a multi-instrument data set was analyzed. Recall which data set were used.*

We added as the new second sentence of the section:

“The multiple instruments used were RPC-LAP, RPC-ICA, RPC-MAG, and RPC-MIP, all part of the Rosetta Plasma Consortium.”

*Line 276: indicate that the waves were recorded as Langmuir probe current variations*

We changed the sentence to read

“Waves which we interpret as current-driven ion acoustic waves were recorded by the Langmuir probe instrument RPC-LAP as probe current variations.”

*Line 283-284: The ion drift value, obtained from the analysis of the LAP I-V curve, was questioned above. What is the process causing the ion drift speed of 3 to 3.7 km/s. Could this be partly a local phenomena inside the sheath of the charged spacecraft?*

Ions are accelerated by an ambipolar field radially outward from the nucleus. The sheath around the spacecraft is not affecting the measurement, as the probe is outside the sheath. In a plasma with a 2eV electron temperature and a  $1.6 \times 10^9 \text{ m}^{-3}$  density, the Debye

length is 26 cm. The probe is therefore outside the sheath. Note that this is an upper limit. Should cold electrons be included, the resulting value would be even lower.

The Debye length estimate compared to the boom length is in the new section on uncertainties, and we added the following text about the acceleration process in the discussion section:

“Theoretical estimates of acceleration by a radial ambipolar electric field lead to ion bulk speeds in this range (Vigren and Eriksson, 2017) in agreement with observations (Odelstad et al., 2018).”

*Line 285: replace “electron volt” by “eV”*

Changed as suggested.

*Line 288: « ... possible to say something about it ». I found this statement very speculative with the limited cases tested.*

We have said something about it, so it is possible. We make no claim of being able to say everything about it. The statement as it stands is not speculative.

*Line 295: remove « the » before « bulk »*

Changed as suggested.

*Line 297: Discuss the processes that would increase the bulk temperature or form supra-thermal tails. Can wave-particle interaction contribute to the ion heating process ?*

Particle populations can absorb energy through wave-particle interaction or by acceleration by dc fields, often followed by wave-particle interaction. However, it is wise not to speculate about matters that we cannot support by measurement.

*Current carried by cold electrons?*

This is part of the list of properties of the distribution that best agrees with the observations:

“It has the warmest cold ion distribution (0.04 eV), the current carried by the cold electrons, and no warm ion component as that was found to be negligible.”

*Line 313-316: Indeed, it seems pretty strong conclusions are reached from crude estimates and measurements with uncertainties (which are not quantified).*

We think that in the amended manuscript, with the newly added discussion of the uncertainties, the conclusions are justified.

# Ion acoustic waves near a comet nucleus: Rosetta observations at comet 67P/Churyumov-Gerasimenko

Herbert Gunell<sup>1</sup>, Charlotte Goetz<sup>2</sup>, Elias Odelstad<sup>3</sup>, Arnaud Beth<sup>1</sup>, Maria Hamrin<sup>1</sup>, Pierre Henri<sup>4,5</sup>, Fredrik L. Johansson<sup>6</sup>, Hans Nilsson<sup>7</sup>, and Gabriella Stenberg Wieser<sup>7</sup>

<sup>1</sup>Department of Physics, Umeå University, 901 87 Umeå, Sweden

<sup>2</sup>Space Research and Technology Centre, European Space Agency, Keplerlaan 1, 2201AZ Noordwijk, The Netherlands

<sup>3</sup>Department of Space and Plasma Physics, Royal Institute of Technology, 100 44 Stockholm, Sweden

<sup>4</sup>LPC2E, CNRS, F-45071 Orléans, France

<sup>5</sup>Lagrange, OCA, CNRS, UCA, Nice, France

<sup>6</sup>Swedish Institute of Space Physics, Box 537, 751 21 Uppsala, Sweden

<sup>7</sup>Swedish Institute of Space Physics, Box 812, 981 28 Kiruna, Sweden

**Correspondence:** Herbert Gunell (herbert.gunell@physics.org)

**Abstract.** Ion acoustic waves were observed between 15 and 30 km from the centre of comet 67P/Churyumov-Gerasimenko by the Rosetta spacecraft during its close flyby on 28 March 2015. There are two electron populations: one cold at  $k_B T_e \approx 0.2 \text{ eV}$  and one warm at  $k_B T_e \approx 4 \text{ eV}$ . The ions are dominated by a cold (a few hundredths of eV) distribution of water group ions with a bulk speed of  $(3\text{--}3.7) \text{ km s}^{-1}$ . A warm  $k_B T_e \approx 6 \text{ eV}$  ion population, which also is present, has no influence on the ion acoustic waves due to its low density of only 0.25 % of the plasma density. Near closest approach the propagation direction was within  $50^\circ$  from the direction of the bulk velocity, leading to a Doppler shift of the waves that in the spacecraft frame. The waves, which in the plasma frame appear below the ion plasma frequency  $f_{pi} \approx 2 \text{ kHz}$ , are Doppler shifted to the spacecraft frame where they cover a frequency range up to approximately 4 kHz. The wave power decreased waves are detected in a region of space where the magnetic field is piled up and draped around the inner part of the ionised coma. Estimates of the current associated with the magnetic field gradient as observed by Rosetta are used as input to calculations of dispersion relations for current-driven ion acoustic waves, using kinetic theory. Agreement between theory and observations is obtained for electron and ion distributions with the properties described above. The wave power decreases over cometocentric distances from 24 to 30 km. The main difference between the plasma at closest approach and in the region where the waves are decaying is the absence of a significant current in the latter. Wave observations and theory combined supplement the particle measurements that are difficult at low energies and complicated by spacecraft charging.

*Copyright statement.* ©The authors 2020. This work is distributed under the Creative Commons Attribution 4.0 License

## 1 Introduction

Observations of waves can give us information of the plasma in which they are generated and through which they have ~~travelled~~propagated. Waves are also of general interest in plasma physics as they provide a means for energy transfer and  
20 because they affect the charged particle distributions through wave–particle interaction processes. When comets 21P/Giacobini-Zinner and 1P/Halley were visited by spacecraft in the 1980s a variety of plasma waves were reported (Scarf et al., 1986c, a; Scarf, 1989). Among these observations were ion acoustic waves, detected both in the bow shock region (Scarf et al., 1986b) and upstream (Oya et al., 1986).

The Rosetta spacecraft (Glassmeier et al., 2007a) accompanied comet 67P/Churyumov-Gerasimenko for two years from  
25 August 2014 to September 2016. Shortly after the spacecraft reached the comet, low frequency ( $f \lesssim 100$  mHz) long wavelength ( $100 \text{ km} \lesssim \lambda \lesssim 700 \text{ km}$ ) waves were detected in the magnetic field data (Richter et al., 2015, 2016). These were named “singing comet” waves; they have been interpreted in terms of a modified ion-Weibel instability (Meier et al., 2016), found to be compressional (Breuillard et al., 2019), and detected as far as 800 km from the nucleus (Goetz et al., 2020). Waves in the lower hybrid frequency range ( $f \lesssim 15$  Hz) were found by André et al. (2017) and Karlsson et al. (2017). Lower hybrid waves were  
30 frequently seen in bursts in connection with density gradients, oscillating on minute time scales (Stenberg Wieser et al., 2017). These minute time scale oscillations are known as steepened waves ~~, and they~~and were observed outside the diamagnetic cavity (Goetz et al., 2016b, a). Electric field measurements showed waves in the lower hybrid frequency range on both sides of the diamagnetic cavity boundary, indicating a mode conversion between lower hybrid waves and ion acoustic waves (Madsen et al., 2018).

35 Ion acoustic waves are compressional plasma waves that are weakly damped only when  $T_e \gg T_i$ , where  $T_e$  and  $T_i$  are the electron and ion temperatures respectively, and the frequency is below the ion plasma frequency. In this limit, the angular frequency  $\omega$  is proportional to the wave number  $k$  and the phase speed is  $c_s = \sqrt{k_B T_e / m_i}$ , where  $k_B$  is Boltzmann’s constant and  $m_i$  is the ion mass (see for example Krall and Trivelpiece, 1973). As the frequency approaches the ion plasma frequency they become increasingly heavily damped and also the phase speed decreases. If the ion and electron temperatures are simi-  
40 lar, this also leads to heavy damping, and ion acoustic waves are usually not detectable in that regime. ~~Ion~~Charged particle distributions become unstable when one population drifts at a large enough speed relative another population, and this results in the growth of waves. In particular, this applies to the current-driven ion acoustic instability, where the electron and ion populations are in relative motion. The current-driven ion acoustic instability has been studied in laboratory experiments (Sato et al., 1976; Kawai et al., 1978; Michelsen et al., 1979), and Stringer (1964) mapped out the unstable parameter regimes  
45 theoretically. At comet 67P/Churyumuov-Gerasimenko ion acoustic waves were observed by the Rosetta spacecraft on 20 January 2015 (Gunell et al., 2017b) at approximately 2.5 AU from the Sun, before the diamagnetic cavity had formed (see Goetz et al., 2016a, f  
, and also in the diamagnetic cavity near perihelion (Gunell et al., 2017a). The ion acoustic waves seen in the cavity were interpreted as a result of part of the current at the diamagnetic cavity boundary closing through bulges on that boundary and generating waves through a current–driven instability (Gunell et al., 2017a). Ion acoustic waves can be identified by measuring  
50 either the variations in plasma density or in the electric field. At comet 67P/Churyumov-Gerasimenko, Gunell et al. (2017b)

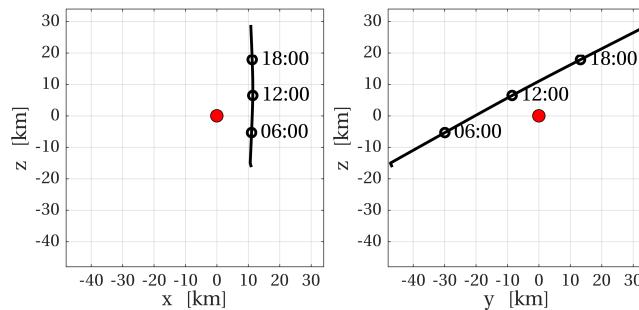


**Figure 1.** Trajectory followed by the Rosetta spacecraft during the close flyby on 28 March 2015. The red circle represents the nucleus of comet 67P/Churyumov-Gerasimenko.

detected the waves in electric field oscillations and Gunell et al. (2017a) in density variations. In this work, the detection relies on density variations.

In this article, we examine ion acoustic waves detected by Rosetta during its close flyby of comet 67P on 28 March 2015. The comet was at a heliocentric distance of 2.0 AU at the time, and the gas production rate varied between  $3 \times 10^{26} \text{ s}^{-1}$  and  $9 \times 10^{26} \text{ s}^{-1}$  during the day. Magnetic pileup and draping ~~has~~ have been studied before for this flyby, both in observational studies and using hybrid simulations (Koenders et al., 2016). The magnetic field piled up near the nucleus, causing the solar wind protons to be deflected out of the ecliptic plane. This in turn caused the draped magnetic field in the region near the nucleus to align itself with the deflected solar wind flow. No sign of a diamagnetic cavity was seen during the flyby, and that was likely due to it not having formed yet (Goetz et al., 2016a). The hybrid simulations of the flyby presented by Koenders et al. (2016) show the presence of an infant bow shock (Gunell et al., 2018) approximately 100 km from the nucleus, but that is farther out than the spacecraft reached on that day. Thus, the spacecraft was situated in the inner coma, where the plasma was of cometary origin. The plasma parameters, although not exactly the same, were in a range similar to that of the diamagnetic cavity observations near perihelion. The magnetic field environment was dominated by magnetic pileup and draping during the flyby, while the diamagnetic cavity has its own peculiar magnetic field environment with a sharp discontinuity at the boundary.

65

## 2 Observations

We use the comet-centred solar equatorial coordinate system (CSEQ) throughout this article. In this system, the  $x$  axis points from the comet to the Sun, the  $z$  axis is the component of the rotation axis of the Sun that is perpendicular to the  $x$  axis, and the  $y$  axis is directed to complete the right-handed coordinate system ~~=(original definition in the SPICE kernel, Acton, 1996)~~. The spacecraft moved from negative to positive  $y$  and  $z$  values at a nearly constant  $x = 11$  km. The spacecraft trajectory is illustrated in Fig. 1.

70

The closest approach occurred at 13:05 UTC, and then Rosetta was at a cometocentric distance of 15 km. The spacecraft moved slowly (with a relative speed to the comet below  $1 \text{ m s}^{-1}$ ) and was in the vicinity of the nucleus for several hours as shown in Fig. 1 and in panel h of Fig. 2.

## 75 2.1 Instrumentation

The data used in this article was obtained by instruments belonging to the Rosetta Plasma Consortium (RPC) (Carr et al., 2007). For the wave observations (Sect. 2.2) we used the Rosetta Langmuir probe instrument (RPC-LAP) (Eriksson et al., 2007) to record time series of ~~plasma-probe current variations attributed to~~ waves in the cometary plasma environment. RPC-LAP is constituted of two spherical probes, 5 cm in diameter, that are mounted on booms protruding from the spacecraft. Starting at 10:55:34 on 28 March 2015, RPC-LAP regularly recorded such time series for the rest of the day. The probe current was sampled at a frequency of  $f_s = 18750 \text{ Hz}$ , and each time series contains 1600 samples, corresponding to a time series length of 85.3 ms. This process was repeated every 160 s. Each of the two probes obtained 295 such time series during the day. The power spectral density for each time series is computed, using Welch's method (Welch, 1967), averaging segments that are 256 samples long with an overlap of 65 % (Fig. 2a and b). The probes were held at fixed potentials with respect to the spacecraft: probe 1 at +30 V and probe 2 at -30 V. For reference, the spacecraft potential was approximately -20 V with respect to the plasma. The Langmuir probe instrument was also used to ~~measure-derive~~ the bulk speed of the ions and the electron temperature by sweeping the probe potential and measuring the probe current as described in Sect. 2.3.

We use the Mutual Impedance Probe (RPC-MIP) (Trotignon et al., 2007) to obtain the plasma density during the flyby. The RPC-MIP instrument observes the plasma frequency, from which the plasma density is derived (Fig. 2f). The ion populations are sampled by the Ion Composition Analyser (RPC-ICA) (Nilsson et al., 2007) (Fig. 2g). The magnetic field is measured by the magnetometer (RPC-MAG) (Glassmeier et al., 2007b). The magnetic field components are presented in CSEQ coordinates in Fig. 2d. How the properties of the plasma are derived from the data collected by these instruments is described in Sect. 2.3.

## 2.2 Waves

Power spectral densities obtained for RPC-LAP probe 1 are shown in Fig. 2a, and those recorded by probe 2 are shown in Fig. 2b. The colour coded quantity is the logarithm of the power spectral density (PSD) of the probe currents. The lowest frequency bins are at risk of picking up low-frequency noise, and we therefore show the spectrum for frequencies above 200 Hz. There may be other waves present at low frequencies, but in this article we only consider ion acoustic waves above 200 Hz. The waves are identified as ion acoustic waves, because they are compressional, showing a plasma density variation, and other wave modes can be excluded for the spatial and temporal scales where they are observed as shown in Sect. 2.4.

100 A high amplitude wave signal is seen during the close flyby and it falls off as the spacecraft moves away from the nucleus. The power spectral density of the positively biased probe 1 is several orders of magnitude higher than that of the negative probe 2. This means that the probe 1 signal is dominated by the electron current and that the signal is proportional to the density variation of the wave. The probe ~~was thus operating in the same regime as when waves were observed-operated in this regime also in the previously published observations of waves~~ in the diamagnetic cavity ~~when the comet was at perihelion~~

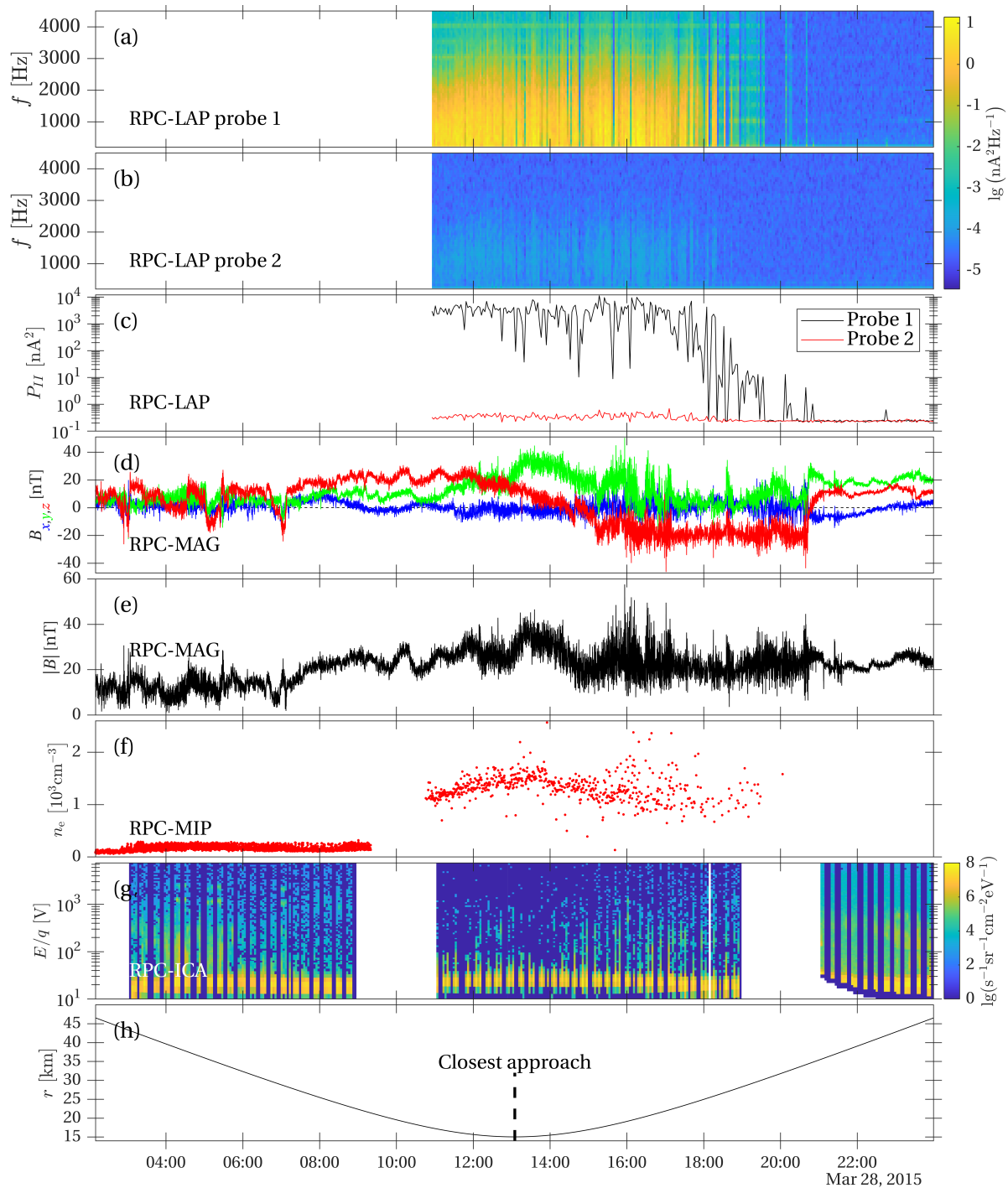


**Figure 2.** Rosetta observations during the close flyby of comet 67P/Churyumov-Gerasimenko on 28 March 2015. **(a)** Power spectral density of RPC-LAP probe 1 in the frequency range  $200 \text{ Hz} < f < 4.5 \text{ kHz}$ . **(b)** Power spectral density of RPC-LAP probe 2 in the same frequency range. **(c)** The power spectral density of probes 1 and 2 integrated from 200 Hz to the Nyquist frequency of 9375 Hz. **(d)** RPC-LAP probe 1 was biased to +30 V and probe 2 was biased to -30 V with respect to the spacecraft potential. **(e)**  $B_x$  (blue),  $B_y$  (green), and  $B_z$  (red) components of the magnetic flux density measured by RPC-MAG. **(f)** The magnitude of the magnetic flux density. **(g)** The plasma density measured by derived from RPC-MIP data. **(h)** Ion energy spectrum observed by RPC-ICA summed over all angles and mass channels. **(i)** Cometocentric distance of the Rosetta spacecraft.

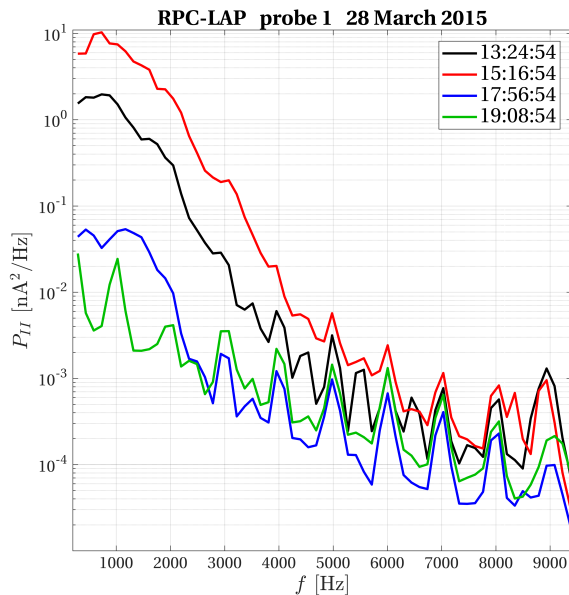


**Figure 3.** Power spectral densities from 200 Hz up to the Nyquist frequency for the RPC-LAP probe 1 current for four different times during the Rosetta close flyby of comet 67P. The black curve (13:24:54) is used in Sect. 3 for analysis of waves near closest approach and the blue curve (17:56:54) for similar analysis of during the outbound part of the flyby.

105 [\(Gunell et al., 2017a\)](#)[\(Gunell et al., 2017a\)](#), whereas in the first published observations [\(Gunell et al., 2017b\)](#), the probe was capacitively coupled to the plasma. A simple test to distinguish between the two regimes is to measure the wave amplitude as a function of probe bias, where a negatively biased probe suppresses the electron current [\(Torvén et al., 1995\)](#). In the present case, we compare the two probes that are biased differently [\(see also Gunell et al., 2017b\)](#). Also the maximum PSD value is similar to those observations and the plasma density, shown here in Fig. 2f, was in both cases somewhat above  $1000\text{cm}^{-3}$ .

110 The situation differs from the first ion acoustic wave observations at comet 67P [\(Gunell et al., 2017b\)](#) when the plasma density was an order of magnitude smaller and the waves coupled capacitively to the probe through the displacement current instead of a particle current. The difference between the probes is also seen in Fig. 2c, which shows the integral of the power spectral density over frequencies from 200 Hz up to the Nyquist frequency.

Fig. 3 shows four sample spectra of the probe 1 current for frequencies from 200 Hz up to the Nyquist frequency. There is wave power starting at the low end of this frequency range with a broad maximum in the vicinity of 1 kHz, and at higher frequencies the PSD declines toward the noise floor. The black curve shows the PSD at 13:24:54, which is near closest approach to the comet nucleus at a cometocentric distance of 15 km. As seen in Fig. 2c the total wave power fluctuated but remained at a generally high level while the spacecraft was in the near-nucleus environment. The PSD obtained at 15:16:54 (red curve in Fig. 3) is another example from this period. The spacecraft was at 17.5 km cometocentric distance and the wave power was even

120 higher than that shown by the black curve. The wave power declined as the spacecraft moved to larger cometocentric distances.

This process started approximately at 17:45 when Rosetta was at 24 km from the centre of the nucleus. Two examples from the declining phase are shown in Fig. 3: the spectrum obtained at 17:56:54 at 25 km (blue curve) and one spectrum from 19:08:54 at 29 km (green curve) when the wave power had fallen even more. The two curves that will be used for comparison with wave theory in Sect. 3 are the black curve (13:24:54) for closest approach and the blue curve (17:56:54) for the outbound case. The peaks at multiples of 1 kHz seen in the frequency range where the wave power is low, both in Fig. 3 and Fig. 2 are artefacts generated by the spacecraft.

### 2.3 Plasma properties

To analyse the waves we need to know the basic properties of the plasma. The plasma density obtained by the mutual impedance probe, RPC-MIP, is shown in Fig. 2f. The density peaks around closest approach and then falls off as the spacecraft moves away from the nucleus. The scattered instantaneous plasma density values are a signature of strong plasma inhomogeneities of approximately 10% around closest approach. For the calculations in Sect. 3 we estimate a plasma density of  $n_e = 1600 \text{ cm}^{-3}$  at closest approach and  $n_e = 1000 \text{ cm}^{-3}$  for the outbound case.

Fig. 2g shows an energy spectrum of the positive ions observed by RPC-ICA. Starting at  $E/q \approx 20 \text{ V}$  is a warm ( $k_B T_i \approx 6 \text{ eV}$  around the time of closest approach) water ion population, which has been accelerated toward the spacecraft due to the negative spacecraft potential. The temperature was obtained by fitting a drifting Maxwellian to the data recorded by the instrument. Some accelerated water ions are seen at higher energies, but the vast majority of the ions seen in Fig. 2g belong to the warm, low energy, population. Fitting the observed flux to a drifting Maxwellian distribution we arrive at a density estimate of about  $4 \text{ cm}^{-3}$  for this ion population. However, this is far below the  $1600 \text{ cm}^{-3}$  plasma density measured by RPC-MIP. ~~It was shown by Bergman et al. (2020a, b) that low energy (down to 5 eV) ions describe complicated orbits in the potential well around the spacecraft. Therefore the field of view of the instrument may be far from what is nominally expected, and the low energy part of the observed distribution functions can be very inaccurate. The field of view for ions with lower energies than the 5 eV lower limit considered by Bergman et al. (2020a, b) is even more limited, and the fraction of that population that is detected may not be distinguishable from ions belonging to the warm population.~~ The sensitivity of RPC-CIA is low in the lowest energy range, and the angular range that allows entry into the instrument is narrow. A mono-energetic low energy beam is liable to be undetected. Thus, the discrepancy between the RPC-ICA measured ion density and the plasma density measured by RPC-MIP may be explained by a cold water ion distribution that is invisible to RPC-ICA.

This is confirmed by Langmuir probe characteristics shown in Fig. 4. ~~The left panel Fig. 4b~~ shows the part of the characteristics dominated by the ion current. In the following we estimate the bulk speed of the cold ions. The warm ion population is negligible because of its low density, and cold plasma theory is applicable because the thermal speed of the cold ions is far below their bulk speed. For a cold ion population drifting at a bulk speed  $u$  the probe current  $I$  depends on the probe to plasma potential  $V$  according to (Mott-Smith and Langmuir, 1926)

$$I = -\pi r_p^2 n_i u e \left( 1 - \frac{2eV}{m_i u^2} \right), \quad (1)$$

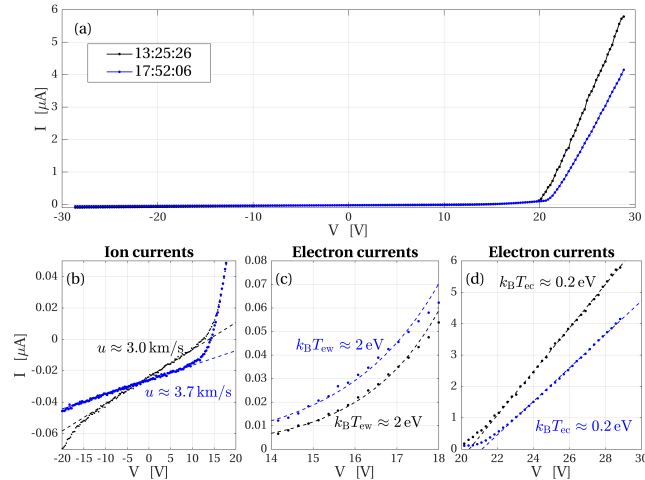


**Figure 4.**  $I$ - $V$  traces from RPC-LAP near closest approach (black) and during the outbound part of the flyby (blue). The left-hand panel shows the (a) complete  $I$ - $V$  traces, (b) ion currents and the right-hand panel current part of the electron currents. The dashed characteristics and lines have been fitted to the  $I$ - $V$  traces ion currents in order to estimate find the bulk speed of the cold ion population. (c) electron currents and exponentials fitted to determine the warm electron temperature. (d) electron saturation current part of the characteristics and lines fitted to determine the temperature of the cold electron population.

where  $r_p = 2.5$  cm is the radius of the probe,  $m_i$  is the ion mass and  $n_i$  the ion density. We fit a line to the linear part of the curve, and taking the derivative of Eq. (1) and rearranging we can determine the drift velocity from the slope  $dI/dV$  of that

155 line:

$$u = \frac{2n_i e^2 \pi r_p^2}{m_i \frac{dI}{dV}}. \quad (2)$$

Taking the ion density to be equal to the plasma density measured by RPC-MIP we arrive at an ion drift speed of  $3 \text{ km s}^{-1}$  near closest approach and  $3.7 \text{ km s}^{-1}$  at 17:52:06 when the spacecraft was moving outward as shown in Fig. 4b. These numbers are within the range of those observed by Odelstad et al. (2018). The velocity obtained from Eq. is an upper limit, as it is based on

160 the assumption of cold, zero temperature, ions in spite of the differences in the magnetic field environment and distance to the nucleus. The ion temperature can be estimated from the neutral temperature, as ions are created by ionisation of the neutrals. Biver et al. (2019) found neutral temperatures in the 50–200 K range, which corresponds to approximately 0.02 eV, and that is well below the 1 eV kinetic energy, corresponding to the 3–3.7  $\text{km s}^{-1}$  drift speeds obtained above.

The right-hand panel of This confirms the assumptions stated above Eq. (1) and ensures the applicability of the equation.

165 Photo emission comes in as an offset in the ion current, below the plasma potential, and as such, does not play a role in the slope of the ion current. Furthermore, for the first of the sweeps, the probe was in shadow behind the spacecraft. The deviation from the linear fit at the low voltage end of Fig. 4b could be caused by secondary emission provoked by impacting ions, but the quantum yield is low for low energies and our analysis of the ion current only starts at -10 V. For the wave analysis, the probe is positively biased, rendering ion impact, and hence also secondary emission, negligible.

170 Fig. 4d shows the part of the probe characteristic where the current is dominated by the electrons. The dashed lines have been fitted to the high probe potential part of the sweep. Here, the current varies linearly with voltage (Swift and Schwar, 1970) and the cold electron temperature is (Engelhardt et al., 2018)

$$T_e = 8\pi \frac{r_p^4 e^3 n_e^2}{m_e} \left( \frac{dI}{dV} \right)^{-2}. \quad (3)$$

The slopes of these lines correspond to temperatures of  $k_B T_e = 0.2 \text{ eV}$  for both the closest approach and outbound curves. 175 The curves also show that the plasma potential is ~~between 12 and 14~~ approximately 20 volts above the spacecraft potential; ~~approximately. For the spacecraft to become that negatively charged there must be an additional electron population which is warmer.~~ It was shown in simulations by Johansson et al. (2020) that the spacecraft potential is driven negative by positively biased elements on the solar panels that collect cold electrons from the plasma. The estimate we use in Sect. 3 is that the electron distribution is constituted by two contributions with equal densities: one cold with temperatures as estimated in Fig. 4d and 180 one warm with a temperature of ~~42~~ 42 eV. ~~This follows~~ The latter is found by fitting exponential curves to the part of the  $I-V$  trace dominated by the warm electrons as shown in Fig. 4c. These results are similar to previous Langmuir probe sweep interpretations from when the comet was near perihelion (Eriksson et al., 2017; Gunell et al., 2017a; Odelstad et al., 2018) with the difference that the cold electrons are not quite as cold here as the 0.1 eV that was estimated near perihelion. These two electron temperature values are within the range of those observed by RPC-MIP at similar heliocentric distances in 2016 185 (Wattiaux et al., 2020). The general instrumental response of the RPC-MIP mutual impedance probe in a plasma characterised by two electron populations with different temperatures is described by Gilet et al. (2017) and Wattiaux et al. (2020).

Figure 2d shows the components and Fig. 2e the magnitude of  $\mathbf{B}$  as measured by RPC-MAG. The magnitude of the magnetic field increased as the spacecraft approached the centre of the comet and decreased as it was moving away. This is expected from magnetic pileup and field line draping, but there are also other changes in the magnetic field that can be seen in Fig. 2d 190 and e.

To estimate the current associated with the non-uniformity of the magnetic field we fit lines to the magnitude of the magnetic field as shown in Fig. 5. ~~Then~~ Assuming that the spacecraft moves through a stationary magnetic field, we estimate the magnitude of the current density by

$$J = \frac{|\Delta B|}{\mu_0 |\Delta \mathbf{r}|}.$$

195

$$J = \frac{|\Delta B|}{\mu_0 |\Delta \mathbf{r}|}. \quad (4)$$

where  $|\Delta B|$  is the change in the fitted magnetic field magnitude and  $|\Delta \mathbf{r}|$  is the distance the spacecraft moved during the same period of time. This yields a current density of  $J = 4.9 \mu\text{A m}^{-2}$  when the spacecraft was approaching the nucleus and  $J = 1.9 \mu\text{A m}^{-2}$  while it was moving away. These values should be seen as estimates of the average current density. Koenders 200 et al. (2016) compared the magnetic field observed during this flyby to the magnetic field obtained in hybrid simulations and

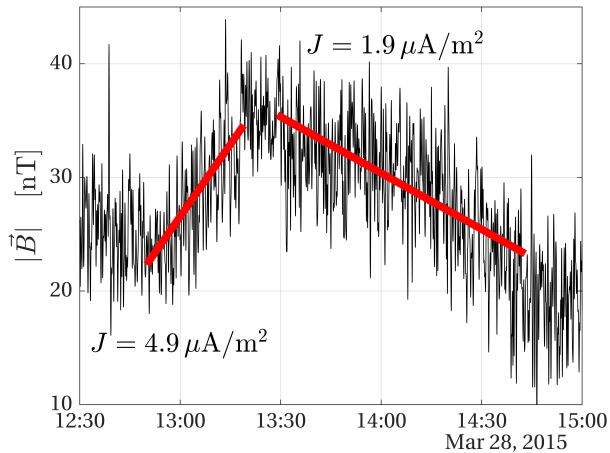


**Figure 5.** Magnetic field magnitude during a period around closest approach. The red lines are fitted to the data in order to derive the current densities  $J = 4.9 \mu\text{A m}^{-2}$  (inbound) and  $J = 1.9 \mu\text{A m}^{-2}$  (outbound).

found good agreement for  $B_y$ , which is the dominating component. The simulated  $B_z$  component was about a factor of 2 lower than what was observed by Rosetta. The difference could be attributed to the limited resolution or the use of an averaged outgassing profile in the simulations (Koenders et al., 2016). For the magnitude of  $\mathbf{B}$  the difference only amounts to 10–20 %, but the simulation does not follow how the plasma quantities develop in time. Fig. 5 shows that the magnetic field changed on much shorter timescales than those of our linear approximations during the flyby. From a single spacecraft measurement we cannot determine whether these magnetic field fluctuations are due to local variations of the current in the plasma or whether the whole inner region of the ionised coma is undergoing oscillations. Thus, the current density may have been both higher and lower than these average values during the flyby.

## 2.4 Typical scales

A plasma density of  $1600 \text{cm}^{-3}$  corresponds to an electron plasma frequency of approximately 350 kHz and a  $\text{H}_2\text{O}^+$  ion plasma frequency of 2 kHz. Thus, electron time scale waves, such as Langmuir waves and electron acoustic waves, are far beyond reach of our observations, the Langmuir probe being sampled at the much lower frequency of 18.75 kHz. Ion acoustic waves, on the other hand, are in the accessible frequency range. The magnetic field during the flyby varied between 20 and 40 nT approximately. This corresponds to electron cyclotron frequencies between 0.6 and 1.1 kHz, which is in the middle of the observed frequency range. However, the observed wave frequency does not follow the changes in the magnetic field, which rules out electron cyclotron waves. For example, the PSD peaks at 700 Hz for both times 13:24:54 and 15:16:54, shown by the black and red curves in Fig. 3, respectively, even though the electron cyclotron frequency was 1.1 kHz at 13:24:54 and 0.57 kHz at 15:16:54. The ion cyclotron frequency is (0.02 – 0.03) Hz, which is below the frequencies we can resolve.

220 The spacecraft was at 15 km cometocentric distance at closest approach and at 25 km at 18:00 when the wave amplitude started to decrease. Thus, the typical length for the variation in wave amplitude is about 10 km. Assuming a typical  $B$  of 30 nT warm ions at 6 eV would have a gyroradius of 50 km. Cold ions are picked up by the electric field, moving along trajectories with a radius of curvature that is even larger. The ions can thus be seen as unmagnetised. Warm electrons at 4 eV have gyroradius of 225 m and for cold 0.2 eV electrons the gyroradius is 50 m approximately.

225 In Sect. 3 we use kinetic theory to compute dispersion relations for electrostatic waves in an unmagnetised plasma. This is applicable if the wavelength is much shorter than the gyroradii of the partieles electrons and ions so that the influence of magnetic forces on particle motion is negligible on wavelength scales. In Sect. 3 it is seen that the phase speed for ion acoustic waves is approximately  $1.7 \text{ km s}^{-1}$ . Thus, a wave at 200 Hz (the lower limit of the spectrum shown in Fig. 2a) has a wavelength of 8.5 m, which is far below all the gyroradii reported above. The assumption that the plasma is unmagnetised for wave purposes holds above that limit, and these are the waves considered here. For waves at the very lowest frequencies, below 230 the range considered here, the wavelength is longer, and electromagnetic effects would have to be taken into account.

## 2.5 Measurement uncertainties

All measurements are associated with uncertainties. The random error of the RPC-MIP derived densities are in the range of 10–20 %. The error is computed from the frequency resolution of the instrument, which measures the plasma frequency line of the mutual impedance spectra. For RPC-MAG the uncertainty in individual measurements is 5 nT (Goetz et al., 2016a). This is less than the natural variations that are seen on the magnetic field curves in Fig. 2. The cold ion population is not detected by RPC-ICA. Ions with energies above a few eV are detected and their energy is known to the precision of the width of the energy bins, which is 30 % at energies below 30 eV. The direction from which the low energy ions arrive at the instrument depends heavily on the electric fields around the spacecraft and it requires modelling to relate the observed arrival directions to the travel directions of ions outside the spacecraft sphere of influence (Bergman et al., 2020a, b). For the very lowest energies the sensitivity is low, and also ions can enter the instrument only from a narrow angular range. For RPC-LAP the uncertainty lies more in the interpretation than in the measurement of currents and voltages. We will now discuss the uncertainties in those interpretations that we have made, using data from all instruments.

235  
240

The spacecraft potential is determined from the Langmuir probe characteristics, and that estimate could be off by  $\sim 2$  eV. This does not affect the slopes of the characteristics that are used to determine the electron cold and warm temperatures as well as the ion drift speed. The temperature of the cold electrons is calculated using Eq. (3). The most significant contribution to error in Eq. (3) is the electron density, which is squared in the equation. We used the density determined by RPC-MIP, which has an error of 10–20 %. The total error in Eq. (3) is estimated to be  $\lesssim 50$  %. The estimate of the warm electron temperature could be influenced by other electron populations. However, the exponential fit ends 2 V below the plasma potential, and the cold electrons have little influence there, given their low 0.2 eV temperature. The probe was in the shadow behind the spacecraft during closest approach, which means that there was no influence from photo electrons. The measurement performed while the spacecraft was outbound could in principle have been influenced by photo electrons, even though no substantial change in temperature was observed. The possible error is estimated to be covered by the 1–4 eV range spanned by the test distributions

245  
250

in Sect. 3. The ion velocity is found by the use of Eq. (2). The velocity is proportional to the density, which is obtained by RPC-MIP, which means that the 10–20% random error in those measurements applies to the velocity as well. Any influence of a spacecraft sheath on the RPC-LAP measurements is negligible, since the probe is outside the sheath. The Debye length in a plasma with a 2 eV electron temperature and a  $1.6 \times 10^9 \text{ m}^{-3}$  density is  $\lambda_{De} = 26 \text{ cm}$ , which is much less than the boom length of 2.24 m. This value of  $\lambda_{De}$  is an upper limit, since it is based on the warm electrons. If the cold electrons would also be included, lower values would be obtained, which would place the probe even farther outside the sheath. Deviations from the nominal value due to density and temperature fluctuations are estimated at less than a factor of 2, and the probe would remain outside the sheath also under such conditions.

The estimate of the warm ion temperature from the RPC-ICA observations is subject to an uncertainty of the order of the spacecraft potential uncertainty  $\sim 2 \text{ eV}$ . The cold ion temperature cannot be measured directly, but it can be confined to below  $\sim 1 \text{ eV}$ , since if the temperature were higher, the high energy tails would be visible in the energy range that can be observed. The wave observations constrain the cold ion temperature further as is seen in the growth rate calculations with different temperature in Sect. 3.

The current density estimate is influenced by the error in the magnetic field measurements and the error in the spacecraft position. The latter can be neglected as it is of the order of tens of metres, and the spacecraft moved  $|\Delta \mathbf{r}| = 2 \text{ km}$  and  $5 \text{ km}$  during inbound and outbound measurement periods, respectively, as shown in Fig. 5. An upper limit of the error of the current density estimate of 40% is obtained if the full 5 nT random error of the individual estimate is applied to  $|\Delta B|$  in Eq. (4).

### 270 3 Dispersion relations

Because of the uncertainty at which both electron and ion distribution functions are known, we have calculated dispersion relations under several different assumptions about these distributions. We then compare the results of the calculations with the wave observations in order both to arrive at an explanation for how the waves are generated and to put constraints on what we can say about the ~~charged particle~~ electron and ion distributions. The total distribution function is composed of a cold and a warm electron and a cold and a warm ion distribution. The parameters are shown in Table 1 for 7–9 test cases used to model the distribution near closest approach and 2 cases for the outbound trajectory. We use the simple pole expansion method to compute the dispersion relations (Löfgren and Gunell, 1997; Gunell and Skiff, 2001, 2002; Tjulin et al., 2000; Tjulin and André, 2002). In a comet context it was reviewed by Gunell et al. (2017b, also providing the computer code for the computations). Each component of the distribution function is modelled by an approximate Maxwellian,

$$280 \quad M_m(v) = \left[ 1 + \frac{(v - v_d)^2 (v - v_D)^2}{2v_t^2} + \dots + \frac{1}{m!} \left( \frac{(v - v_d)^2 (v - v_D)^2}{2v_t^2} \right)^m \right]^{-1}, \quad (5)$$

where  $v$  is velocity,  $v_t$  is the thermal speed,  $v_d - v_D$  is the drift speed, and  $m$  is the number of terms included in the expansion. The procedure used to calculate dispersion relations is briefly described in Appendix A. The expression inside the brackets of

**Table 1.** Parameters of the distributions used in the examples related to the plasma at closest approach. In the table,  $n$  means density,  $k_B$  is Boltzmann's constant,  $T$  denotes temperature, and  $v_D$  represents drift speed.

distr.	cold ions			warm ions			cold electrons			warm electrons		
	$n$ [cm <sup>-3</sup> ]	$k_B T$ [eV]	$v_D$ [km s <sup>-1</sup> ]	$n$ [cm <sup>-3</sup> ]	$k_B T$ [eV]	$v_D$ [km s <sup>-1</sup> ]	$n$ [cm <sup>-3</sup> ]	$k_B T$ [eV]	$v_D$ [km s <sup>-1</sup> ]	$n$ [cm <sup>-3</sup> ]	$k_B T$ [eV]	$v_D$ [km s <sup>-1</sup> ]
Closest approach												
1	1554	0.02	0	4	6	0	779	0.2	39.3	779	<u>4.2</u>	0
2	1558	0.02	0	0	–	–	779	0.2	39.3	779	<u>4.2</u>	0
3	1518	0.02	0	40	6	0	779	0.2	39.3	779	<u>4.2</u>	0
4	1558	0.02	0	0	–	–	779	0.2	0	779	<u>4.2</u>	39.3
5	1558	0.02	0	0	–	–	779	0.2	39.3	779	1	0
6	1558	0.01	0	0	–	–	779	0.2	39.3	779	<u>4.2</u>	0
7	1558	0.04	0	0	–	–	779	0.2	39.3	779	<u>2</u>	<u>0</u>
<u>8</u>	<u>1558</u>	<u>0.02</u>	<u>0</u>	<u>0</u>	<u>–</u>	<u>–</u>	<u>779</u>	<u>0.2</u>	<u>39.3</u>	<u>779</u>	4	0
<u>9</u>	<u>1558</u>	<u>0.02</u>	<u>0</u>	<u>0</u>	<u>–</u>	<u>–</u>	<u>779</u>	<u>0.2</u>	<u>19.6</u>	<u>779</u>	<u>2</u>	<u>19.6</u>
Outbound												
A	1006	0.02	0	0	–	–	503	0.2	23.6	503	<u>4.2</u>	0
B	1006	0.02	0	0	–	–	503	0.2	0	503	<u>4.2</u>	0

Eq. (5) is the reciprocal of a Taylor expansion of

$$\exp\left(\left(v - v_{\text{dD}}\right)^2 / (2v_{\text{t}}^2)\right).$$

285 As  $m$  tends to infinity  $M_m(v)$  approaches a Maxwellian, and for small values of  $m$  the distributions have suprathermal tails. In the distributions in Table 1,  $m = 3$  for the ions and  $m = 5$  for the electrons. The influence of suprathermal tails is evaluated in Appendix [??B](#).

Fig. 6. shows dispersion relations for the [7–9](#) test cases that correspond to the observations near closest approach. We are assuming a real wave number  $k$  and a complex angular frequency  $\omega$ . Panel (a) shows the real part of  $\omega$ , and panel (b) shows the damping rate  $\gamma$ . Negative values of  $\gamma$  correspond to wave growth. Panel (c) shows the shaded rectangle in panel (b) in more detail. Several of the curves are so similar they fall on top of each other and are difficult to distinguish in the figure. In all cases the least damped or fastest growing mode is the ion acoustic mode and that is the one shown.

The density of the warm ion population is varied in distributions 1–3. In distribution 1 the warm ion density is 4 cm<sup>-3</sup> as estimated in Sect. 2.3. In distribution 2 the warm ion density is assumed to be zero, and in distribution 3 the warm ion density is ten times higher than the estimate in Sect. 2.3. The real part of the dispersion relation is indistinguishable among the three cases, as seen in Fig. 6a. The damping rates in Fig. 6c are very close in the three cases, although it can be described that

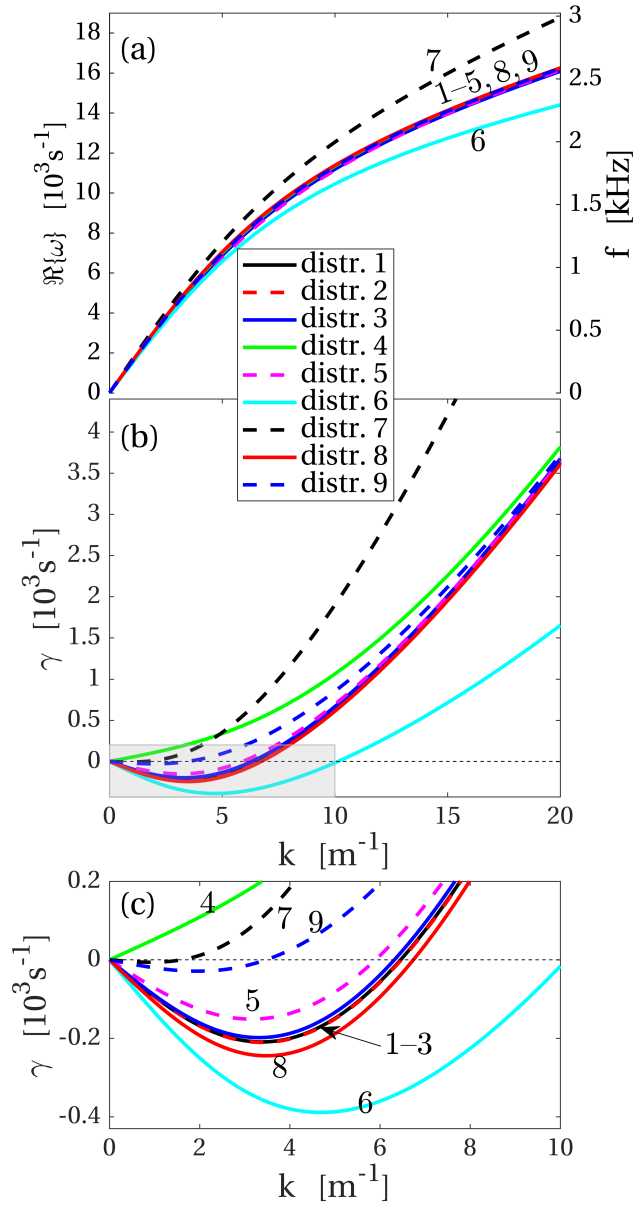


**Figure 6.** Dispersion relations at closest approach for the seven assumed distributions specified in Table 1. (a)-(a) real part of the dispersion relation. (b)-(b) damping rate  $\gamma$ . (c)-(c) zoom-in on the shaded rectangle in panel (b). The numbers next to the curves identify the different distribution functions shown in Table 1. Positive values of  $\gamma$  correspond to wave damping and negative values to wave growth.

distribution 3, with the highest warm ion density, has a slightly smaller growth rate than the other two. However, the difference is small, and we conclude that the warm ion population only has a negligible influence on the waves. Therefore, the warm ion density is set to zero in the rest of the distribution functions.

300 We have used the current density estimate,  $J = 4.9 \mu\text{A m}^{-2}$ , obtained in Sect. 2.3 for the inbound part of the flyby. The dispersion relations are computed in the rest frame of the ions and the current is modelled by assigning a drift velocity,  $|\mathbf{v}_D| = 39.3 \text{ km s}^{-1}$   $|\mathbf{v}_D| = |J/(en)| = 39.3 \text{ km s}^{-1}$ , to one of the electron populations. Here,  $n$  denotes the density of the electron population in question. In distribution 2 and distribution 4 that drift speed is given to the cold and warm electron distribution, respectively. For distribution 4 the ion acoustic mode is damped, while it is growing for distribution 2. We conclude  
305 that to drive the ion acoustic waves unstable the current must not be carried by the ~~cold electrons~~ warm electrons alone. In distribution 9 the current is carried by both electron populations, which each are given a drift velocity of  $|\mathbf{v}_D| = 19.6 \text{ km s}^{-1}$ . This yields a lower growth rate than for distribution 2, but the mode is still unstable for a range of  $k$  values.

In distribution 5, the temperature of the warm electrons has been decreased to 1 eV. This leads to a decreased growth rate compared to distribution 2, which has 42 eV warm electrons but otherwise is equal to distribution 5. In distribution 8 the electron temperature has been increased to 4 eV with all other parameters the same as in distributions 2 and 5. The growth rate for distribution 8 is higher than that for the other two distributions. However, in ~~both all three~~ cases the waves are unstable over ~~approximately the same a similar~~ wavelength range.

Distributions 6 and 7 have 0.01 eV and 0.04 eV cold ions, respectively, that is to say, in distribution 6 the ions are colder and in distribution 7 warmer than they are in the otherwise equal distribution 2. This affects the growth rate so that distributions  
315 with colder ions grow faster and over a wider  $k$  range than distributions where the ions are warmer (Fig. 6c). Also the real part of  $\omega$  is affected, as shown in Fig. 6a, but this is significant only for  $k$  values larger than the  $k$  which corresponds to maximum growth. The influence of suprathermal ~~particles~~ ions on the dispersion relations and growth rates is evaluated in Appendix ~~??~~ B, and it is found to be similar to the difference between distribution with 0.01 and 0.02 eV ions. The distribution function of the cold ions cannot be measured directly, and hence effects caused by the shape of the distribution cannot be distinguished from  
320 effects caused by the temperature alone. However, we may conclude from all ~~7-9~~ cases that any process that gives the ions higher or the electrons lower energy will lead to decreased growth or increased damping.

Dispersion relations for distributions A and B, detailed in Table 1, are shown in Fig. 7. These distributions correspond to the plasma parameters obtained during the outbound passage of the spacecraft, and close to when the PSD represented by the blue line in Fig. 3 was recorded at 17:56:54. In distribution A the cold electrons have been given a drift velocity corresponding to the  
325 current density  $J = 1.9 \mu\text{A m}^{-2}$  measured when the spacecraft was moving away, and the dispersion relation corresponding to distribution A is very similar to those at closest approach. In distribution B none of the populations have been assigned a drift velocity. This leads to a stable distribution, and the waves are weakly damped instead of growing. Examining the magnetic field in Fig. 2 we see no large scale change near 18:00, which 00. That the field remains constant, except for small fluctuations, while the spacecraft moves means that there ~~was~~ is no large scale magnetic field gradient in this region and hence no large  
330 scale current present either. Thus, the change in the plasma that affects the waves is the absence of a current, and this indicates that the reason why the wave spectrum fades out as the spacecraft moves away from the nucleus is the decline of the current

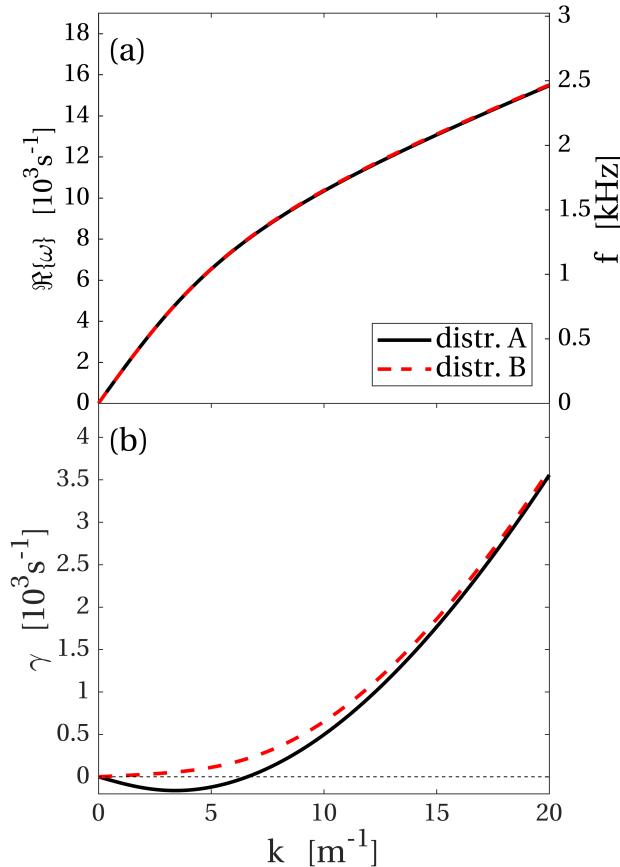


**Figure 7.** Dispersion relations while the spacecraft was outward bound based on assumed distributions specified in Table 1. (a)-(a) real part of the dispersion relation. (b)-(b) damping rate  $\gamma$ . Positive values of  $\gamma$  correspond to wave damping and negative values to wave growth.

density. Around 18:00 the waves likely were propagating to the spacecraft from a source region closer to the nucleus, where the current density was still high enough to generate the waves.

#### 4 Doppler shift

335 The dispersion relations are computed in the ion frame of reference and the observations are, by necessity, performed in a spacecraft-fixed frame. A frequency  $f_m$  in the moving medium is Doppler shifted to frequency  $f_{sc}$  in the spacecraft frame according to

$$f_{sc} = \frac{v_{ph}(f_m) + u \cos(\alpha)}{v_{ph}(f_m)} f_m, \quad (6)$$

where  $v_{ph}$  is the phase velocity given by the dispersion relation,  $u$  is the speed of the moving medium, and  $\alpha$  is the angle  
 340 between the wave direction of propagation and the velocity  $\mathbf{u}$ . Fig. 8a shows the  $\text{H}_2\text{O}^+$  ion plasma frequency and the frequency

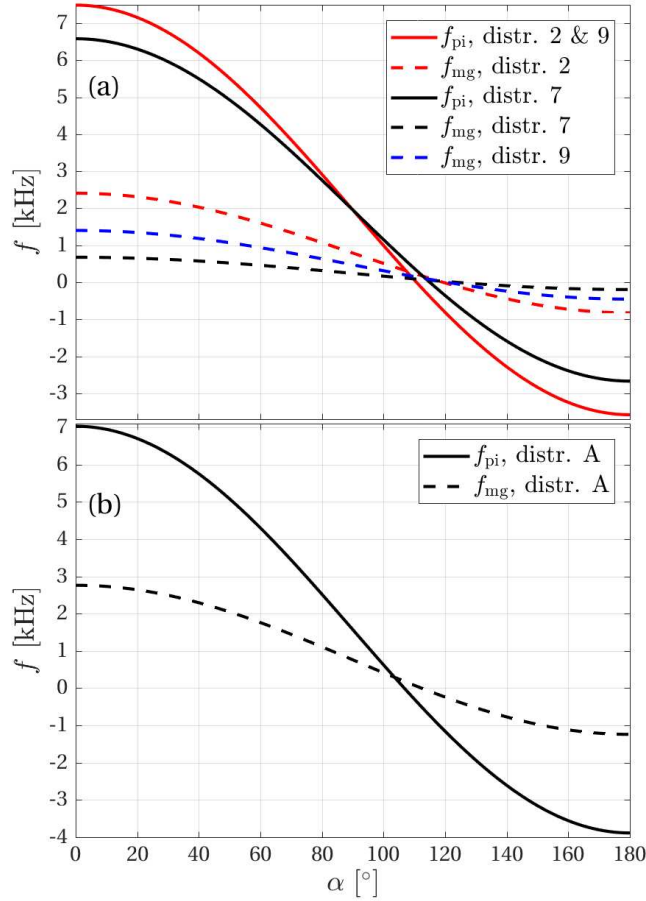


**Figure 8.** Doppler shifted  $\text{H}_2\text{O}^+$  ion plasma frequencies,  $f_{pi}$  and frequencies of maximum growth (a),  $f_{mg}$ , (a) at closest approach and (b) (b) during the outbound motion of the spacecraft. The dispersion relations used to compute the Doppler shift correspond to distributions 2, 7, 9, and A in Table 1.

of maximum growth, Doppler shifted to the spacecraft frame according to Eq. (6) for the dispersion relations that correspond to distributions 2 and 7, 7 and 9, and with  $u$  determined by Eq. (2). The frequencies are shown as functions of the angle  $\alpha$ . The angle is not known from observations, but by comparing the Doppler shifted frequencies to the observed spectrum we can assess what values of  $\alpha$  would lead to a reasonable spectrum an interpretation in which observations and theory are consistent.

345 This is explained in what follows.

The dispersion relations show that the damping is considerable at the ion plasma frequency. This has also been seen in experiments with current-driven ion acoustic waves, where the power declines with frequency and reaches the noise floor at frequencies well below the ion plasma frequency (Kawai et al., 1978). For our near closest approach sample spectrum shown by the black curve in Fig. 3 this happens at approximately 5 kHz. The range of angles  $\alpha$  consistent with the observed spectra

350 can then be constrained to those for which the ion plasma frequency is mapped to frequencies above 5 kHz. If the waves follow the dispersion relation corresponding to [distribution distributions 2 or 9](#), (solid red curve in Fig. 8a) this means that  $\alpha \lesssim 56^\circ$  and in the case of distribution 7 (solid black curve in Fig. 8a) the angle is restricted to  $\alpha \lesssim 48^\circ$   $\alpha \lesssim 49^\circ$ . We will round this off to  $\alpha \lesssim 50^\circ$ .

For a particular dispersion relation to be in agreement with observations, there should be significant wave power at the  
355 Doppler shifted frequency of maximum growth. With this regard distribution 7 is in better agreement with observations than distribution 2, because the spectrum has fallen significantly at 2 kHz and the dashed red curve in Fig. 8a is above 2 kHz for most of the relevant angle range of  $\alpha \lesssim 50^\circ$  determined above. The dashed black curve is close to 1 kHz in this range, and it is in good agreement with the peak of the spectrum in Fig. 3. [The dashed blue curve corresponding to the frequency of maximum growth for distribution 9, in which cold and warm electrons both carry current in equal measure, falls between the](#)  
360 [the other two.](#) Of the different dispersion relations we have examined it is the one corresponding to distribution 7 that best fits the Rosetta data. However, several distributions can lead to similar growth rates at similar frequencies, and we cannot constrain the distribution function closely. What we can say is that distributions that lead to moderate growth rates are in better agreement with the data than those that show very rapid growth.

[For the outbound part of the spacecraft trajectory,](#) Fig. 8b shows the Doppler shifted ion plasma frequency and frequency of  
365 maximum growth for distribution A. The real part of the dispersion relation for distributions A and B overlap in Fig. 7, and therefore the Doppler shifted ion plasma frequency will be the same for distribution B as for distribution A. For distribution B the waves are damped everywhere, and there is no frequency of maximum growth. We have already concluded in Sect. 3 that distribution B is more likely than distribution A, and that the waves that were observed as the spacecraft moved away were not generated at the spacecraft location. The frequency where the wave power peaks tells us more about the source region than  
370 about the conditions at the spacecraft position. The blue curve in Fig. 3 has fallen to the noise floor at approximately 3 kHz, and from the solid curve in Fig. 8b the dispersion relation is seen to be in agreement with data for angles in the range  $\alpha \lesssim 70^\circ$ .

## 5 Discussion and conclusions

We have analysed data obtained during Rosetta's close flyby of comet 67P on 28 March 2015. [The multiple instruments used were RPC-LAP, RPC-ICA, RPC-MAG, and RPC-MIP, all part of the Rosetta Plasma Consortium.](#) Waves which we  
375 interpret as current-driven ion acoustic waves were recorded by the Langmuir probe instrument RPC-LAP [as probe current variations.](#) These waves were seen all the time the spacecraft was close to the nucleus and the wave power started to decrease at approximately 24 km cometocentric distance. We estimated the current density from magnetic field measurements and found that the same currents that are involved in draping and pileup of the magnetic field (Koenders et al., 2016) are sufficient to drive the ion acoustic mode unstable, according to the kinetic model we have used to compute dispersion relations. Koenders  
380 et al. (2016) could observe field line draping until the rapid magnetic field change that occurred at 20:42 when Rosetta was at 34 km cometocentric distance.

Data from RPC-LAP indicate the presence of two electron populations, one cold at temperature around 0.2 eV and one warm at  $\sim 4$  eV. Furthermore, the RPC-LAP characteristics show the presence of a cold ion population drifting with a speed between  $3 \text{ km s}^{-1}$  and  $3.7 \text{ km s}^{-1}$ . This-Theoretical estimates of acceleration by a radial ambipolar electric field lead to ion bulk speeds in this range (Vigren and Eriksson, 2017) in agreement with observations (Odelstad et al., 2018). The cold component of the ion distribution went undetected by the ion spectrometer RPC-ICA. Instead a warm, several ~~electron volts~~ eV in temperature, ion distribution was detected by RPC-ICA, but its density is not sufficient for it to have any significant influence on the waves.

We are not able to measure the fine details of the ~~partiele~~ electron and ion distributions. However, by testing different assumptions about the distributions it is possible to say something about it. We have seen that the best agreement between the theoretical dispersion relations and the observed wave spectra is obtained when the growth rate is moderate. This can be achieved with a cold ion distribution with  $k_B T = 0.04 \text{ eV}$ . This is the warmest cold distribution that we tried, but it is still a very low temperature compared to all the other charged particle populations. The same result may be obtained with a lower temperature, if there also are suprathermal ~~partieles~~ ions present. To accurately measure distribution functions at such low energies would represent a challenge in space-based instrumentation. These cold ion temperatures are reasonable, considering that Biver et al. (2019) found neutral temperatures up to approximately 0.02 eV between the nucleus and 15 km cometocentric distance. The ion distribution is formed by ionisation of the neutrals, and initially the neutral and ion temperatures are the same. On their way out to the spacecraft position, the ions may undergo some heating either through an increased ~~the~~ bulk temperature or by forming suprathermal tails. The rapidly decreased growth with increasing cold ion temperature from 0.01 via 0.02 to 0.04 eV also shows that the cold ion temperature is of this order (a few hundredths eV). For a warmer cold ion population, the distribution would be stable and no waves generated, and as seen in Sect. 4, if the cold ion population is 0.01 eV or colder the higher growth rate leads to a worse agreement with observations. The growth rate is also influenced by what fraction of the current is carried by the cold electrons. This, in turn, depends on the relative speed of the two electron populations and how the electron density is distributed between them. To summarise the result of computing dispersion relations for ~~different distributions~~ the different distributions we have tried, it is distribution 7 in Table 1 that shows the best agreement with observations. It has the warmest cold ion distribution (0.04 eV), the current carried by the cold electrons, and no warm ion component as that was found to be negligible.

By computing the Doppler shift and comparing observed spectra with wave theory and known properties of current-driven ion acoustic waves we can estimate the angle between the bulk velocity of the cold ions and the propagation direction of the waves to be  $\alpha \lesssim 50^\circ$  for closest approach and  $\alpha \lesssim 70^\circ$  farther out when Rosetta was moving away and the wave power decreasing. Previous estimates have shown that ions move away from the centre of the comet, predominantly in a radial direction (Odelstad et al., 2018) as would be expected if they are accelerated by the ambipolar field present in the inner coma (Gunell et al., 2019). There are also observations of ions with an anti-sunward velocity component (Berčič et al., 2018), but those ions were faster than the  $(3\text{--}3.7) \text{ km s}^{-1}$  we have observed here. If we assume that the ions move radially outward, the estimate of  $\alpha \lesssim 50^\circ$  for the waves near closest approach will also apply to the angle between the direction of propagation and the radial direction. Waves should propagate in the direction of the relative velocity between the electrons and the ions, and our angle estimates must not be seen as general results. They apply only at the position of the spacecraft during the flyby and

for the orientation of the current at the time. During the outbound pass of the spacecraft, the angle of propagation cannot be restricted more than to say that it is below  $70^\circ$ . Here, Rosetta was likely outside the source region, and the waves propagated to the spacecraft from a source located closer to the nucleus.

420 ~~We~~ The use of wave observations in combination with wave theory complements the other measurements, particularly the cold ion population that is inaccessible to the particle instruments. It also lets us confirm the interpretation of probe data concerning the electron populations, and the interpretation of the observed variation of the magnetic field as a spatial gradient. Yet we only have information about the waves along a single spacecraft trajectory, and what we know about the current comes from crude estimates based on single spacecraft magnetic field observations. To obtain a more complete picture of currents and  
 425 waves in the inner coma would require the comet to be accompanied by multiple spacecraft collecting data at the same time (Götz et al., 2019).

*Code and data availability.* The Rosetta data sets are available at the ESA Planetary Science Archive <<https://archives.esac.esa.int/psa>>. The specific data set used in this article is available at <<https://doi.org/10.5281/zenodo.3973232>> together with computer codes to produce the figures (Gunell et al., 2020).

#### 430 **Appendix A: ~~The influence of suprathermal particles~~Dispersion relations**

In order to compute dispersion relations, the distributions described by Eq. (5) are written as a sum:

$$f(v) = \sum_j \frac{a_j}{v - b_j}, \quad (\text{A1})$$

where  $b_j$  are the poles of the distribution function and  $a_j$  are the residues at those poles. The dielectric function for a plasma containing different species,  $\alpha$ , is (e.g. Krall and Trivelpiece, 1973)

$$435 \quad \epsilon(k, \omega) = 1 + \sum_\alpha \frac{\omega_{p\alpha}^2}{k^2} \int \frac{k df_\alpha(u)/du}{\omega - ku} du. \quad (\text{A2})$$

We normalise each population  $f_\alpha$  and in Eq. (A2) it is weighted with its plasma frequency squared,  $\omega_{p\alpha}^2$ . When integrating in the complex plane, the integral path is closed in the upper half plane, and  $\epsilon(k, \omega)$  is expressed as (Gunell and Skiff, 2002)

$$\epsilon(k, \omega) = 1 - 2\pi i \sum_\alpha \omega_{p\alpha}^2 \sum_{b_{j,\alpha} \in U} \frac{a_{j,\alpha}}{(\omega - kb_{j,\alpha})^2}, \quad (\text{A3})$$

where  $U$  denotes the upper half-plane. We assume a real value for  $k$  and seek a complex  $\omega$  by solving the equation for the  
 440 dispersion relation, which is

$$\epsilon(k, \omega) = 0. \quad (\text{A4})$$

This equation is solved numerically by seeking solutions that minimise  $|\epsilon(k, \omega)|^2$ . For more information about the method the reader is referred to the original articles (Löfgren and Gunell, 1997; Gunell and Skiff, 2001, 2002; Tjulin et al., 2000; Tjulin and André, 2017) and to the short review in a comet context by Gunell et al. (2017b).

#### 445 **Appendix B: The influence of suprathermal ions**

As mentioned in the main text the index  $m$  controls the thickness of the suprathermal tails of the distribution function. In distributions ~~1-7~~1-9,  $m = 3$  for the ions and  $m = 5$  for the electrons. For comparison we have performed calculations with  $m = 6$  and  $m = 8$  for all populations. These are shown in Fig. B1 as distributions ~~8 and 9~~10 and 11 by the red and blue curve respectively. In both cases the cold ion temperature was 0.02 eV, and for comparison the dispersion relation for distribution 6, which has 0.01 eV cold ions, is also shown in Fig. B1. The results are very similar, and we conclude that the influence on the dispersion relation from the suprathermal tails is similar to the difference between distributions with 0.01 and 0.02 eV ions. Since we cannot directly measure the distribution function at these low energies we cannot tell the two effects apart. The distributions with higher  $m$  indices shown in Fig. B1 and those in Fig. 6 both agree with observations within the limits of experimental uncertainty.

455 *Author contributions.* HG performed the analysis in collaboration with CG, who also was the one to identify the flyby as an item of interest for wave studies, and EO, who in particular contributed to the plasma characterisation based on Langmuir probe data. All authors contributed to the writing of the final manuscript.

*Competing interests.* The authors declare that they have no competing interests.

*Acknowledgements.* This work was supported by the Swedish National Space Agency (grants 96/15 and 108/18). CG was supported by an  
460 ESA Research Fellowship. Work at LPC2E/CNRS was supported by CNES and by ANR under the financial agreement ANR-15-CE31-0009-01.

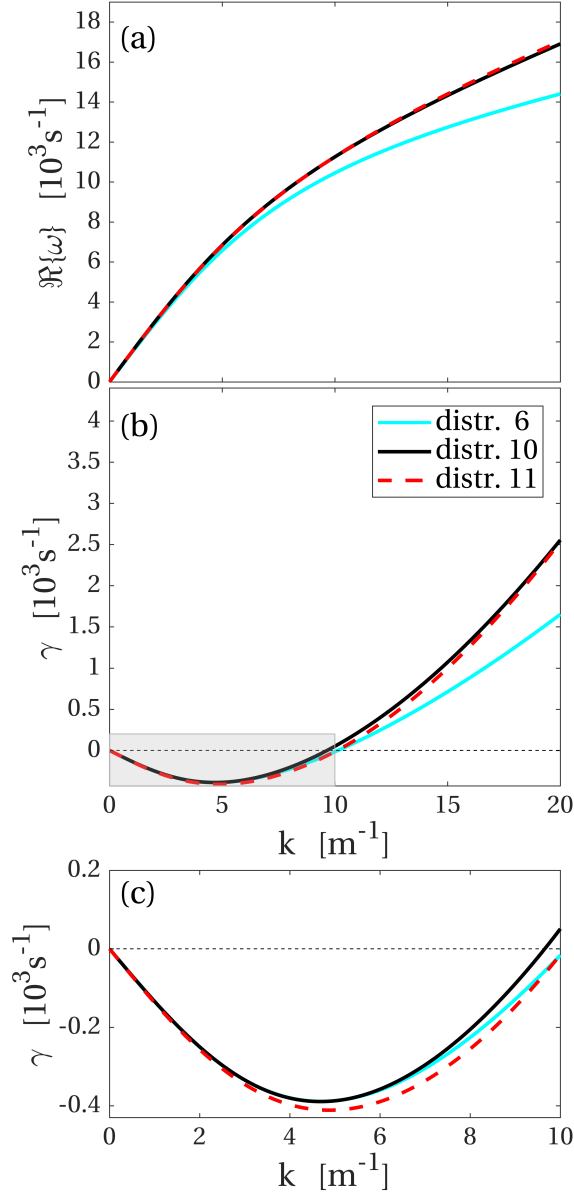


**Figure B1.** Dispersion relations for distributions with different suprathermal tails. Distribution 6 is the same as the distribution with that number shown in Fig. 6, and it has  $m = 3$  for the ions and  $m = 5$  for each of the two electron populations. Distribution 8-10 has  $m = 6$  and distribution 9-11  $m = 8$  for all three populations. (a)-(a) real part of the dispersion relation. (b)-(b) damping rate  $\gamma$ . (c)-(c) zoom-in on the shaded rectangle in panel (b). Positive values of  $\gamma$  correspond to wave damping and negative values to wave growth.

## References

- [Acton, C. H.: Ancillary data services of NASA's Navigation and Ancillary Information Facility, \*Planet. Space Sci.\*, 44, 65–70, 1996.](https://doi.org/10.1016/0032-0633(95)00107-7)
- 465 André, M., Odelstad, E., Graham, D. B., Eriksson, A. I., Karlsson, T., Stenberg Wieser, G., Vigren, E., Norgren, C., Johansson, F. L., Henri, P., Rubin, M., and Richter, I.: Lower hybrid waves at comet 67P/Churyumov-Gerasimenko, *Monthly Notices of the Royal Astronomical Society*, 469, S29–S38, <https://doi.org/10.1093/mnras/stx868>, 2017.
- Berčič, L., Behar, E., Nilsson, H., Nicolaou, G., Stenberg Wieser, G., Wieser, M., and Goetz, C.: Cometary ion dynamics observed in the close vicinity of comet 67P/Churyumov-Gerasimenko during the intermediate activity period, *Astronomy & Astrophysics*, 613, A57, 470 <https://doi.org/10.1051/0004-6361/201732082>, 2018.
- Bergman, S., Stenberg Wieser, G., Wieser, M., Johansson, F. L., and Eriksson, A.: The Influence of Spacecraft Charging on Low-Energy Ion Measurements Made by RPC-ICA on Rosetta, *J. Geophys. Res. (Space Physics)*, 125, e2019JA027478, <https://doi.org/10.1029/2019JA027478>, 2020a.
- Bergman, S., Stenberg Wieser, G., Wieser, M., Johansson, F. L., and Eriksson, A.: The Influence of Varying Spacecraft Potentials and Debye Lengths on In Situ Low-Energy Ion Measurements, *J. Geophys. Res. (Space Physics)*, 125, e2020JA027870, 475 <https://doi.org/10.1029/2020JA027870>, 2020b.
- Biver, N., Bockelée-Morvan, D., Hofstadter, M., Lellouch, E., Choukroun, M., Gulikis, S., Crovisier, J., Schloerb, F. P., Rezac, L., von Allmen, P., Lee, S., Leyrat, C., Ip, W. H., Hartogh, P., Encrenaz, P., Beaudin, G., and the MIRO Team: Long-term monitoring of the outgassing and composition of comet 67P/Churyumov-Gerasimenko with the Rosetta/MIRO instrument, *Astronomy & Astrophysics*, 480 630, A19, <https://doi.org/10.1051/0004-6361/201834960>, 2019.
- Breuillard, H., Henri, P., Bucciattini, L., Volwerk, M., Karlsson, T., Eriksson, A., Johansson, F., Odelstad, E., Richter, I., Goetz, C., Vallières, X., and Hajra, R.: The properties of the singing comet waves in the 67P/Churyumov–Gerasimenko plasma environment as observed by the Rosetta mission, *Astronomy & Astrophysics*, <https://doi.org/10.1051/0004-6361/201834876>, 2019.
- Carr, C., Cupido, E., Lee, C. G. Y., Balogh, A., Beek, T., Burch, J. L., Dunford, C. N., Eriksson, A. I., Gill, R., Glassmeier, K. H., Goldstein, 485 R., Lagoutte, D., Lundin, R., Lundin, K., Lybakk, B., Michau, J. L., Musmann, G., Nilsson, H., Pollock, C., Richter, I., and Trotignon, J. G.: RPC: The Rosetta Plasma Consortium, *Space Science Reviews*, 128, 629–647, <https://doi.org/10.1007/s11214-006-9136-4>, 2007.
- Engelhardt, I. A. D., Eriksson, A. I., Vigren, E., Vallières, X., Rubin, M., Gilet, N., and Henri, P.: Cold electrons at comet 67P/Churyumov-Gerasimenko, *Astronomy & Astrophysics*, 616, A51, <https://doi.org/10.1051/0004-6361/201833251>, 2018.
- Eriksson, A. I., Boström, R., Gill, R., Åhlén, L., Jansson, S.-E., Wahlund, J.-E., André, M., Mälkki, A., Holtet, J. A., Lybakk, B., 490 Pedersen, A., and Blomberg, L. G.: RPC-LAP: The Rosetta Langmuir Probe Instrument, *Space Science Reviews*, 128, 729–744, <https://doi.org/10.1007/s11214-006-9003-3>, 2007.
- Eriksson, A. I., Engelhardt, I. A. D., André, M., Boström, R., Edberg, N. J. T., Johansson, F. L., Odelstad, E., Vigren, E., Wahlund, J.-E., Henri, P., Lebreton, J.-P., Miloch, W. J., Paulsson, J. J. P., Wedlund, C. S., Yang, L., Karlsson, T., Broiles, T., Mandt, K., Carr, C. M., Galand, M., Nilsson, H., and Norberg, C.: Cold and warm electrons at comet 67P/Churyumov-Gerasimenko, *Astronomy & Astrophysics*, 495 605, A15, <https://doi.org/10.1051/0004-6361/201630159>, 2017.
- [Gilet, N., Henri, P., Wattiaux, G., Cilibrasi, M., and Béghin, C.: Electrostatic Potential Radiated by a Pulsating Charge in a Two-Electron Temperature Plasma, \*Radio Science\*, 52, 1432–1448, <https://doi.org/10.1002/2017RS006294>, 2017.](https://doi.org/10.1002/2017RS006294)

- Glassmeier, K.-H., Boehnhardt, H., Koschny, D., Kührt, E., and Richter, I.: The Rosetta Mission: Flying Towards the Origin of the Solar System, *Space Science Reviews*, 128, 1–21, <https://doi.org/10.1007/s11214-006-9140-8>, 2007a.
- 500 Glassmeier, K.-H., Richter, I., Diedrich, A., Musmann, G., Auster, U., Motschmann, U., Balogh, A., Carr, C., Cupido, E., Coates, A., Rother, M., Schwingenschuh, K., Szegő, K., and Tsurutani, B.: RPC-MAG The Fluxgate Magnetometer in the ROSETTA Plasma Consortium, *Space Science Reviews*, 128, 649–670, <https://doi.org/10.1007/s11214-006-9114-x>, 2007b.
- Goetz, C., Koenders, C., Hansen, K. C., Burch, J., Carr, C., Eriksson, A., Frühauff, D., Güttler, C., Henri, P., Nilsson, H., Richter, I., Rubin, M., Sierks, H., Tsurutani, B., Volwerk, M., and Glassmeier, K. H.: Structure and evolution of the diamagnetic cavity at comet  
505 67P/Churyumov-Gerasimenko, *Monthly Notices of the Royal Astronomical Society*, 462, S459, <https://doi.org/10.1093/mnras/stw3148>, 2016a.
- Goetz, C., Koenders, C., Richter, I., Altwegg, K., Burch, J., Carr, C., Cupido, E., Eriksson, A., Güttler, C., Henri, P., Mokashi, P., Nemeth, Z., Nilsson, H., Rubin, M., Sierks, H., Tsurutani, B., Vallat, C., Volwerk, M., and Glassmeier, K.-H.: First detection of a diamagnetic cavity at comet 67P/Churyumov-Gerasimenko, *Astronomy & Astrophysics*, 588, A24, <https://doi.org/10.1051/0004-6361/201527728>, 2016b.
- 510 Goetz, C., Plaschke, F., and Taylor, M. G. G. T.: Singing Comet Waves in a Solar Wind Convective Electric Field Frame, *Geophysical Research Letters*, 47, e2020GL087418, <https://doi.org/10.1029/2020GL087418>, 2020.
- Götz, C., Gunell, H., Volwerk, M., Beth, A., Eriksson, A., Galand, M., Henri, P., Nilsson, H., Wedlund, C. S., Alho, M., Andersson, L., Andre, N., De Keyser, J., Deca, J., Ge, Y., Glaßmeier, K.-H., Hajra, R., Karlsson, T., Kasahara, S., Kolmasova, I., LLera, K., Madanian, H., Mann, I., Mazelle, C., Odelstad, E., Plaschke, F., Rubin, M., Sanchez-Cano, B., Snodgrass, C., and Vigren, E.: Cometary Plasma  
515 Science – A White Paper in response to the Voyage 2050 Call by the European Space Agency, arXiv e-prints, arXiv:1908.00377, <https://arxiv.org/pdf/1908.00377.pdf>, 2019.
- Gunell, H. and Skiff, F.: Weakly damped acoustic-like ion waves in plasmas with non-Maxwellian ion distributions, *Physics of Plasmas*, 8, 3550–3557, <https://doi.org/10.1063/1.1386428>, 2001.
- Gunell, H. and Skiff, F.: Electrostatic fluctuations in plasmas with distribution functions described by simple pole expansions, *Physics of  
520 Plasmas*, 9, 2585–2592, <https://doi.org/10.1063/1.1476666>, 2002.
- Gunell, H., Goetz, C., Eriksson, A., Nilsson, H., Simon Wedlund, C., Henri, P., Maggiolo, R., Hamrin, M., De Keyser, J., Rubin, M., Stenberg Wieser, G., Cessateur, G., Dhooghe, F., and Gibbons, A.: Plasma waves confined to the diamagnetic cavity of comet 67P/Churyumov-Gerasimenko, *Monthly Notices of the Royal Astronomical Society*, 469, S84, <https://doi.org/10.1093/mnras/stx1134>, 2017a.
- Gunell, H., Nilsson, H., Hamrin, M., Eriksson, A., Odelstad, E., Maggiolo, R., Henri, P., Vallières, X., Altwegg, K., Tzou, C.-Y., Rubin, M., Glassmeier, K.-H., Stenberg Wieser, G., Simon Wedlund, C., De Keyser, J., Dhooghe, F., Cessateur, G., and Gibbons, A.:  
525 Ion acoustic waves at comet 67P/Churyumov-Gerasimenko – Observations and computations, *Astronomy & Astrophysics*, 600, A3, <https://doi.org/10.1051/0004-6361/201629801>, 2017b.
- Gunell, H., Goetz, C., Simon Wedlund, C., Lindkvist, J., Hamrin, M., Nilsson, H., LLera, K., Eriksson, A., and Holmström, M.: The infant bow shock: a new frontier at a weak activity comet, *Astronomy & Astrophysics*, 619, L2, <https://doi.org/10.1051/0004-6361/201834225>,  
530 2018.
- Gunell, H., Lindkvist, J., Goetz, C., Nilsson, H., and Hamrin, M.: Polarisation of a small-scale cometary plasma environment: Particle-in-cell modelling of comet 67P/Churyumov-Gerasimenko, *Astronomy & Astrophysics*, 631, A174, <https://doi.org/10.1051/0004-6361/201936004>, 2019.
- Gunell, H., Goetz, C., Odelstad, E., Beth, A., Hamrin, M., Henri, P., Johansson, F. L., Nilsson, H., and Wieser, G. S.: Dataset for Waves  
535 during Rosetta’s close flyby of comet 67P, <https://doi.org/10.5281/zenodo.3973232>, 2020.

- [Johansson, F. L., Eriksson, A. I., Gilet, N., Henri, P., Wattiaux, G., Taylor, M. G. G. T., Imhof, C., and Cipriani, F.: A charging model for the Rosetta spacecraft, \*Astronomy & Astrophysics\*, 642, A43, <https://doi.org/10.1051/0004-6361/202038592>, 2020.](https://doi.org/10.1051/0004-6361/202038592)
- Karlsson, T., Eriksson, A. I., Odelstad, E., André, M., Dickeli, G., Kullen, A., Lindqvist, P.-A., Nilsson, H., and Richter, I.: Rosetta measurements of lower hybrid frequency range electric field oscillations in the plasma environment of comet 67P, *Geophys. Res. Lett.*, 44, 1641–1651, <https://doi.org/10.1002/2016GL072419>, 2017.
- Kawai, Y., Hollenstein, C., and Guyot, M.: Ion acoustic turbulence in a large-volume plasma, *Physics of Fluids*, 21, 970–974, <https://doi.org/10.1063/1.862340>, 1978.
- Koenders, C., Goetz, C., Richter, I., Motschmann, U., and Glassmeier, K.-H.: Magnetic field pile-up and draping at intermediately active comets: results from comet 67P/Churyumov-Gerasimenko at 2.0 AU, *Monthly Notices of the Royal Astronomical Society*, 462, S235–S241, <https://doi.org/10.1093/mnras/stw2480>, 2016.
- Krall, N. A. and Trivelpiece, A. W.: *Principles of Plasma Physics*, McGraw-Hill, New York, 1973.
- Löfgren, T. and Gunell, H.: Flexible Simple-Pole Expansion of Distribution Functions, *Physics of Plasmas*, 4, 3469–3476, <https://doi.org/10.1063/1.872243>, 1997.
- Madsen, B., Simon Wedlund, C., Eriksson, A., Goetz, C., Karlsson, T., Gunell, H., Spicher, A., Henri, P., Vallières, X., and Miloch, W.: Extremely low-frequency waves inside the diamagnetic cavity of comet 67P/Churyumov-Gerasimenko, *Geophys. Res. Lett.*, 45, 3854–3864, <https://doi.org/10.1029/2017GL076415>, 2018.
- Meier, P., Glassmeier, K.-H., and Motschmann, U.: Modified ion-Weibel instability as a possible source of wave activity at Comet 67P/Churyumov-Gerasimenko, *Annales Geophysicae*, 34, 691–707, <https://doi.org/10.5194/angeo-34-691-2016>, 2016.
- [Michelsen, P., Pecseli, H. L., Juul Rasmussen, J., and Schrittwieser, R.: The current-driven, ion-acoustic instability in a collisionless plasma, \*Plasma Physics\*, 21, 61–73, <https://doi.org/10.1088/0032-1028/21/1/005>, 1979.](https://doi.org/10.1088/0032-1028/21/1/005)
- Mott-Smith, H. M. and Langmuir, I.: The Theory of Collectors in Gaseous Discharges, *Physical Review*, 28, 727–763, <https://doi.org/10.1103/PhysRev.28.727>, 1926.
- Nilsson, H., Lundin, R., Lundin, K., Barabash, S., Borg, H., Norberg, O., Fedorov, A., Sauvaud, J.-A., Koskinen, H., Kallio, E., Riihelä, P., and Burch, J. L.: RPC-ICA: The Ion Composition Analyzer of the Rosetta Plasma Consortium, *Space Science Reviews*, 128, 671–695, <https://doi.org/10.1007/s11214-006-9031-z>, 2007.
- Odelstad, E., Eriksson, A. I., Johansson, F. L., Vigren, E., Henri, P., Gilet, N., Heritier, K. L., Vallières, X., Rubin, M., and André, M.: Ion Velocity and Electron Temperature Inside and Around the Diamagnetic Cavity of Comet 67P, *J. Geophys. Res. (Space Physics)*, 123, 5870–5893, <https://doi.org/10.1029/2018JA025542>, 2018.
- Oya, H., Morioka, A., Miyake, W., Smith, E. J., and Tsurutani, B. T.: Discovery of cometary kilometric radiations and plasma waves at comet Halley, *Nature*, 321, 307–310, <https://doi.org/10.1038/321307a0>, 1986.
- Richter, I., Koenders, C., Auster, H.-U., Frühauff, D., Götz, C., Heinisch, P., Perschke, C., Motschmann, U., Stoll, B., Altwegg, K., Burch, J., Carr, C., Cupido, E., Eriksson, A., Henri, P., Goldstein, R., Lebreton, J.-P., Mokashi, P., Nemeth, Z., Nilsson, H., Rubin, M., Szegö, K., Tsurutani, B. T., Vallat, C., Volwerk, M., and Glassmeier, K.-H.: Observation of a new type of low-frequency waves at comet 67P/Churyumov-Gerasimenko, *Annales Geophysicae*, pp. 1031–1036, <https://doi.org/10.5194/angeo-33-1031-2015>, 2015.
- Richter, I., Auster, H.-U., Berghofer, G., Carr, C., Cupido, E., Fornaçon, K.-H., Goetz, C., Heinisch, P., Koenders, C., Stoll, B., Tsurutani, B. T., Vallat, C., Volwerk, M., and Glassmeier, K.-H.: Two-point observations of low-frequency waves at 67P/Churyumov-Gerasimenko during the descent of PHILAE: comparison of RPCMAG and ROMAP, *Annales Geophysicae*, 34, 609–622, <https://doi.org/10.5194/angeo-34-609-2016>, 2016.

- [Sato, N., Popa, G., Märk, E., Mravlag, E., and Schrittwieser, R.: Instability as a source for traveling ion waves, \*Physics of Fluids\*, 19, 70–73, 1976.](https://doi.org/10.1063/1.861330)
- 575 <https://doi.org/10.1063/1.861330>, 1976.
- Scarf, F.: Plasma wave observations at Comets Giacobini-Zinner and Halley, Washington DC American Geophysical Union Geophysical Monograph Series, 53, 31–40, <https://doi.org/10.1029/GM053p0031>, 1989.
- Scarf, F. L., Coroniti, F. V., Kennel, C. F., Sanderson, T. R., Wenzel, K. P., Hynds, R. J., Smith, E. J., Bame, S. J., and Zwickl, R. D.: ICE plasma wave measurements in the ion pick-up region of comet Halley, *Geophys. Res. Lett.*, 13, 857–860, 580 <https://doi.org/10.1029/GL013i008p00857>, 1986a.
- Scarf, F. L., Ferdinand, V., Coroniti, V., Kennel, C. F., Gurnett, D. A., Ip, W.-H., and Smith, E. J.: Plasma wave observations at comet Giacobini-Zinner, *Science*, 232, 377–381, <https://doi.org/10.1126/science.232.4748.377>, 1986b.
- Scarf, F. L., Ferdinand, V., Coroniti, V., Kennel, C. F., Gurnett, D. A., Ip, W.-H., and Smith, E. J.: Plasma wave observations at comet Giacobini-Zinner, *Science*, 232, 377–381, <https://doi.org/10.1126/science.232.4748.377>, 1986c.
- 585 Stenberg Wieser, G., Odelstad, E., Nilsson, H., Wieser, M., Goetz, C., Karlsson, T., Kalla, L., André, M., Eriksson, A. I., Nicolaou, G., Simon Wedlund, C., Richter, I., and Gunell, H.: Investigating short time-scale variations in cometary ions around comet 67P, *Monthly Notices of the Royal Astronomical Society*, 469, S522–S534, <https://doi.org/10.1093/mnras/stx2133>, 2017.
- [Stringer, T. E.: Electrostatic instabilities in current-carrying and counterstreaming plasmas, \*Journal of Nuclear Energy\*, 6, 267–279, 1964.](https://doi.org/10.1088/0368-3281/6/3/305)
- <https://doi.org/10.1088/0368-3281/6/3/305>, 1964.
- 590 Swift, J. D. and Schwar, M. J. R.: *Electrical Probes for Plasma Diagnostics*, Iliffe Books, London, 1970.
- Tjulin, A. and André, M.: The dielectric tensor of simple-pole distribution functions in magnetized plasmas, *Physics of Plasmas*, 9, 1775–1784, <https://doi.org/10.1063/1.1463410>, 2002.
- Tjulin, A., Eriksson, A. I., and André, M.: Physical interpretation of the Padé approximation of the plasma dispersion function, *Journal of Plasma Physics*, 64, 287–296, <https://doi.org/10.1017/S0022377800008606>, 2000.
- 595 [Torvén, S., Gunell, H., and Brenning, N.: A high frequency probe for absolute measurements of electric fields in plasmas, \*Journal of Physics D: Applied Physics\*, 28, 595–599, 1995.](https://doi.org/10.1088/0022-3727/28/3/023)
- <https://doi.org/10.1088/0022-3727/28/3/023>, 1995.
- Trotignon, J. G., Michau, J. L., Lagoutte, D., Chabassière, M., Chalumeau, G., Colin, F., Décréau, P. M. E., Geiswiler, J., Gille, P., Gard, R., Hachemi, T., Hamelin, M., Eriksson, A., Laakso, H., Lebreton, J. P., Mazelle, C., Randriamboarison, O., Schmidt, W., Smit, A., Telljohann, U., and Zamora, P.: RPC-MIP: the Mutual Impedance Probe of the Rosetta Plasma Consortium, *Space Science Reviews*, 128, 600 713–728, <https://doi.org/10.1007/s11214-006-9005-1>, 2007.
- [Vigren, E. and Eriksson, A. I.: A 1D Model of Radial Ion Motion Interrupted by Ion–Neutral Interactions in a Cometary Coma, \*The Astronomical Journal\*, 153, 150, 2017.](https://doi.org/10.3847/1538-3881/aa6006)
- <https://doi.org/10.3847/1538-3881/aa6006>, 2017.
- Wattieaux, G., Henri, P., Gilet, N., Vallières, X., and Deca, J.: Plasma characterization at comet 67P between 2 and 4 AU from the Sun with the RPC-MIP instrument, *Astronomy & Astrophysics*, 638, A124, <https://doi.org/10.1051/0004-6361/202037571>, 2020.
- 605 Welch, P. D.: The Use of Fast Fourier Transform for the Estimation of Power Spectra: A Method Based on Time Averaging Over Short, Modified Periodograms, *IEEE Trans. Audio and Electroacoust.*, AU–15, 70–73, 1967.